Geochemistry and mineralogy of Paleocene-Eocene Oum El Khecheb phosphorites (Gafsa-Metlaoui Basin) Tunisia

Inès Galfati, A. Béji Sassi, A. Zaïer, Jean Luc Bouchardon, Essaïd Bilal, Jean-Louis Joron, Sonia Sassi

G chemical Journal, Vol. 44, pp. 189 to 210, 2010

Geochemistry and mineralogy of Paleocene–Eocene Oum El Khecheb phosphorites (Gafsa–Metlaoui Basin) Tunisia

I. GALFATI,[1,4]* A. BÉJI SASSI,[1] A. ZAÏER,[1] J. L. BOUCHARDON,[2] E. BILAL,[2] J. L. JORON[3] and S. SASSI[1]

[1]Laboratoire des Réssources Minérales et Environnement, Faculté des Sciences, Campus Universitaire, 1060 Tunis, Tunisia
[2]Département Géochimie et Procédés de l'Environnement, Ecole Nationale Supérieure des Mines, 158 Cours Fauriel, 42023 Saint Etienne, France
[3]Laboratoire Pierre Süe, CEA/Saclay, 91191 Gif-sur-Yvette cedex, France
[4]Laboratoire de Géoénergie, Centre de Recherches et des Technologies de l'Energie, Technopole Borj Cédria - 2050 Hammam-Lif, Tunisia

(*Received June 9, 2009; Accepted September 10, 2009*)

Upper Paleocene to Lower Eocene phosphates of the Jebel Oum El Khecheb profile (Gafsa–Metlaoui Basin GMB, Tunisia) are mostly composed of brown phospharenites lithified or not, granular, with pellets, coproliths, bone clasts and fish teeth. The matrix in analyzed samples is reduced and constituted of various clay minerals (dominantly smectites, palygorskite, sepiolite and rare kaolinite), opal-CT and carbonates. Clinoptilolite is recognized along the series; very few amounts of quartz and feldspar grains are sparsely present. The phosphate mineral is a carbonate-fluorapatite (CFA) sulphated, sodic enriched in strontium and rare earth elements (REE). Statistical analyses of mineralogical and geochemical data highlight the associated elements in the main mineral lattice. In the CFA, the group is composed of CaO–P_2O_5–Na_2O–SO_3–F–Sr–Th–REE–U–Ba–Zr–Cr. In the silicates, the group contains SiO_2–Al_2O_3–Fe_2O_3–MgO–K_2O–Na_2O–TiO_2–Co–Cs–Rb–Sc–Ta–Sb–Mo–As and Cu. Sulphides are represented by Zn and Cd; iron oxides by mainly Fe and Ni. Dolomite and gypsum are present; SO_3 is contained in the latter, but CFA may also have some of this radical in its structure. The Upper Continental Crust (UCC) normalized REE patterns present a variably negative Ce-anomaly, suggesting that the imprint of the marine genesis environment is very well-preserved in the main phosphatic units. Positive-Eu and negative-Sm anomalies were detected in some samples. The fractionation of light-REE to heavy-REE, represented by the La/Yb ratio of untreated values varies between 8.28 and 12.94, somewhat less than UCC value (13.64). Enrichment of HREE is due to phosphates. Both ratios reflect the marine genesis environment wherein the formation of the CFA took place in a confined and oxygen poor environment. Then the CFA removed the REE and the trace elements present from the interstitial waters, as was proposed for the various phosphatic basins of Tunisia.

Keywords: phosphorites, carbonate-fluorapatite, REE, trace elements, Tunisia

INTRODUCTION

Trace element contents of phosphorites, such as Sr, U, and rare earth elements (REE), vary from one deposit to another (McKelvey, 1950; Gulbdransen, 1966; Altschuler *et al.*, 1967; Tooms and Summerhayes, 1968; Bliskovsky *et al.*, 1969; Sassi, 1974; Altschuler, 1980; Béji Sassi, 1984; Tlig *et al.*, 1987; Fleet *et al.*, 1997; Soudry *et al.*, 2002). According to these authors, the observed variations are related to: (i) the availability of trace elements in sea water and/or interstitial water in the sedimentary basins (Tooms *et al.*, 1969); and (ii) the cationic substitution capacity of apatite (Sin'Kova *et al.*, 1968; Tooms *et al.*, 1969; Price and Calvert, 1978; Altschuler, 1980; McClellan, 1980; Nathan, 1984; Béji Sassi, 1984, 1999; Béji Sassi *et al.*, 2005; Iqdari *et al.*, 2003).

Rare earth element occurrences were widely studied by previous authors (e.g., Semenov *et al.*, 1962; Altschuler, 1980; Béji Sassi, 1984; Jarvis *et al.*, 1994; Dalirau, 2002; Kidder *et al.*, 2003; Gnandi and Tobschall, 2003) to explain the variable contents and distribution of these key elements in such economically important sediments.

In Tunisia, phosphate deposits are encountered in several localities. However, the Gafsa–Metlaoui Basin located in the southern part of Central Tunisia has been the focus of most of the phosphate-related studies in Tunisia (Visse, 1952; Sassi, 1974, 1980; Chaabani, 1978, 1995; Ben Abdesslem, 1979; Belayouni, 1983; Béji Sassi, 1984, 1999; Tlig *et al.*, 1987; Zaïer, 1984, 1995, 1999; Zaïer *et al.*, 1998; Béji Sassi *et al.*, 2005; and Ounis *et al.*, 2008). These authors described the geology, mineralogy,

*Corresponding author (e-mail: galfatibenromdhane@gmail.com)

geochemistry and palynology of phosphate deposition. To our knowledge, the Jebel Oum El Khecheb, located in the Gafsa–Metlaoui Basin was not the subject of previous mineralogical and/or geochemical investigations. Therefore, our present study focuses on the mineralogical-petrological characteristics of these phosphorites, their associated trace element and REE distribution, which provide invaluable insights to the reconstruction of phosphate genesis and paleoenvironment.

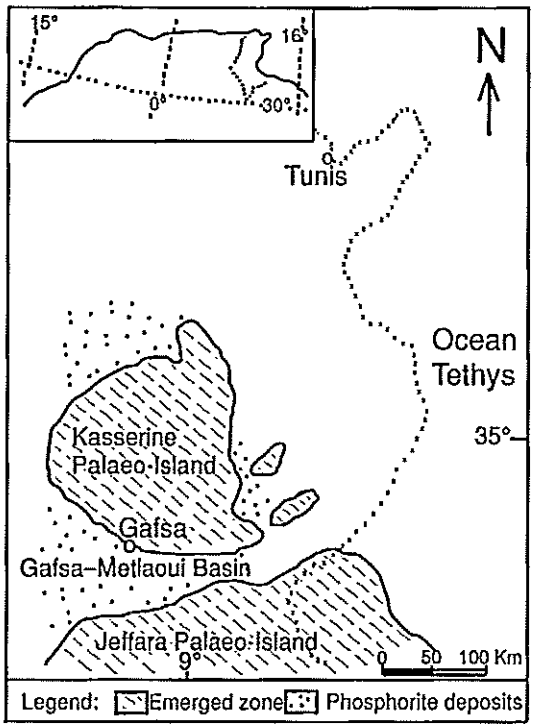

Fig. 1. Paleogeographic map of Tunisia during the Upper Palaeocene–Lower Eocene.

Geology

Regional geological and palaeogeographic context

Phosphorite deposition in Tunisia took place during the Upper Paleocene to Lower Eocene (Fig. 1) within sheltered structures, favorable to the formation and accumulation of the mineral-bearing particles (Sassi, 1974; Chaabani, 1978, 1995; Béji Sassi, 1984; Zaïer, 1995, 1999). The Gafsa–Metlaoui Basin (GMB) constitutes the largest and the most extended deposit phosphate ore mined in Tunisia. The standard section in the GMB profile-type recognizes ten phosphate-rich layers numbered C0 to CIX. A noticeable marker, the chert deposit is located between the CVI and CVII layers.

Local geological context

The anticline of Oum El Khecheb is a secondary fold of Jbel Stah (Fig. 2), located twenty kilometers SW of Gafsa city. It is a short and narrow anticline 11 km length long and 1.5 km wide roughly symmetrical with an ENE-W-SW axis (Sassi, 1974). Synthetical lithostratigraphic chart of Tertiary Tunisian deposits is showed in the left part of Fig. 3.

- The Haria argillaceous Formation (about 50 m thick), Maastrichtian–Paleocene.

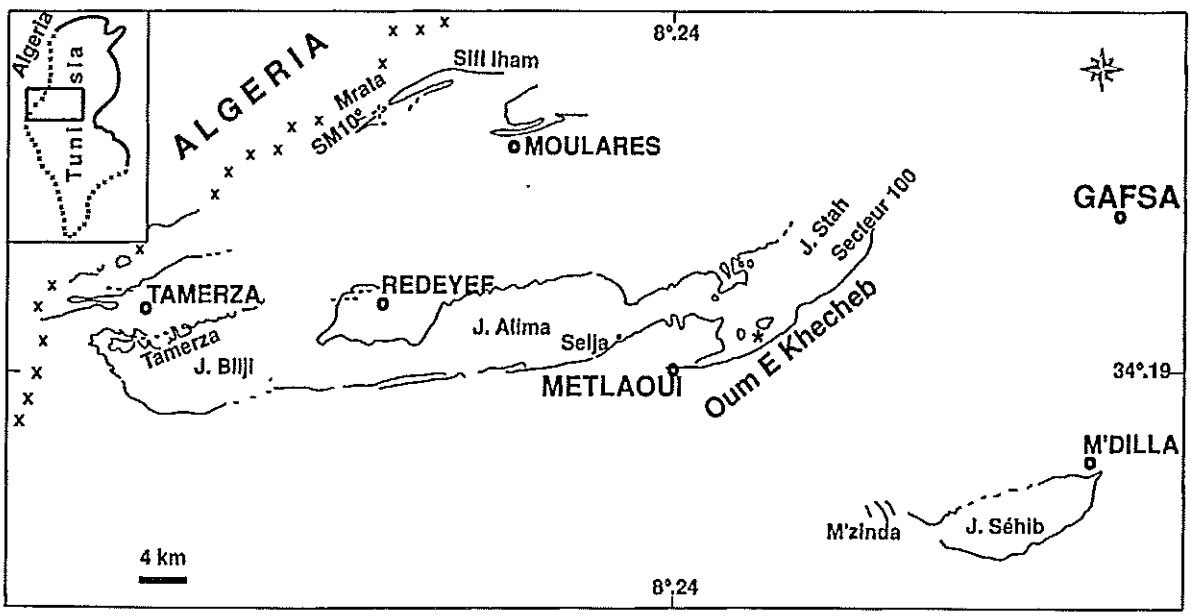

Fig. 2. Outcrops of Phosphatic Series from Gafsa–Metlaoui Basin (GMB) and location of the Oum El Khecheb profile (Tunisia).

- The Metlaoui Formation divided into 3 members:
  - A lower carbonate and evaporitic member (about 85 m thick), dated as Paleocene (Selja member);
  - The middle main phosphatic Chouabine member (35 m in thickness, attributed to the Upper Paleocene) represented by nine phosphatic deposits interbedded with carbonates, clays and a cherty level;
  - The upper carbonate member, comprising bioclastic limestones (50 m), covered by a phosphatic recurrence (4 m) named "the Upper Phosphate", and

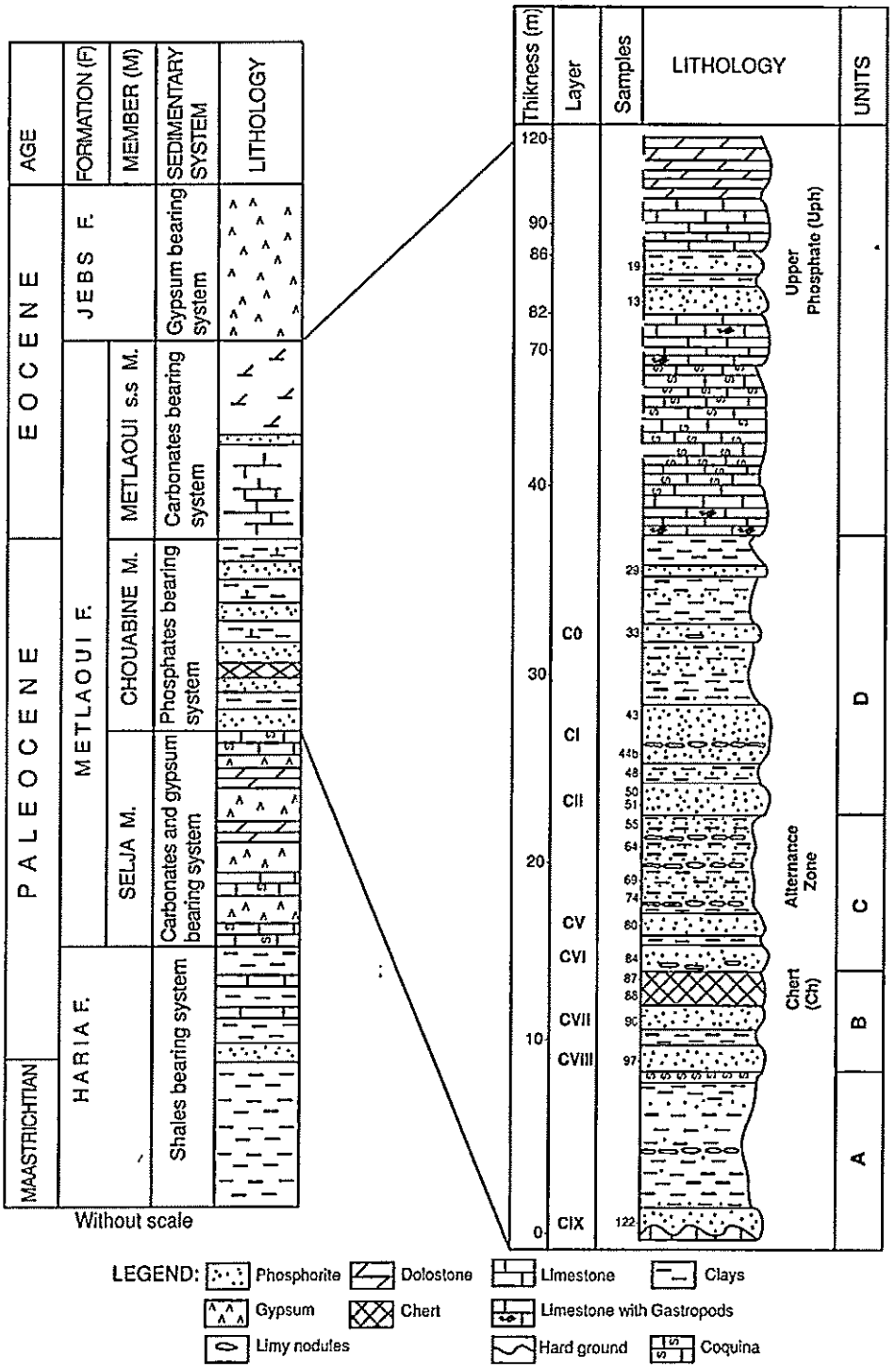

Fig. 3. Lithostratigraphic section of the Paleocene–Eocene sequence of Oum El Khecheb transect (GMB, Tunisia).

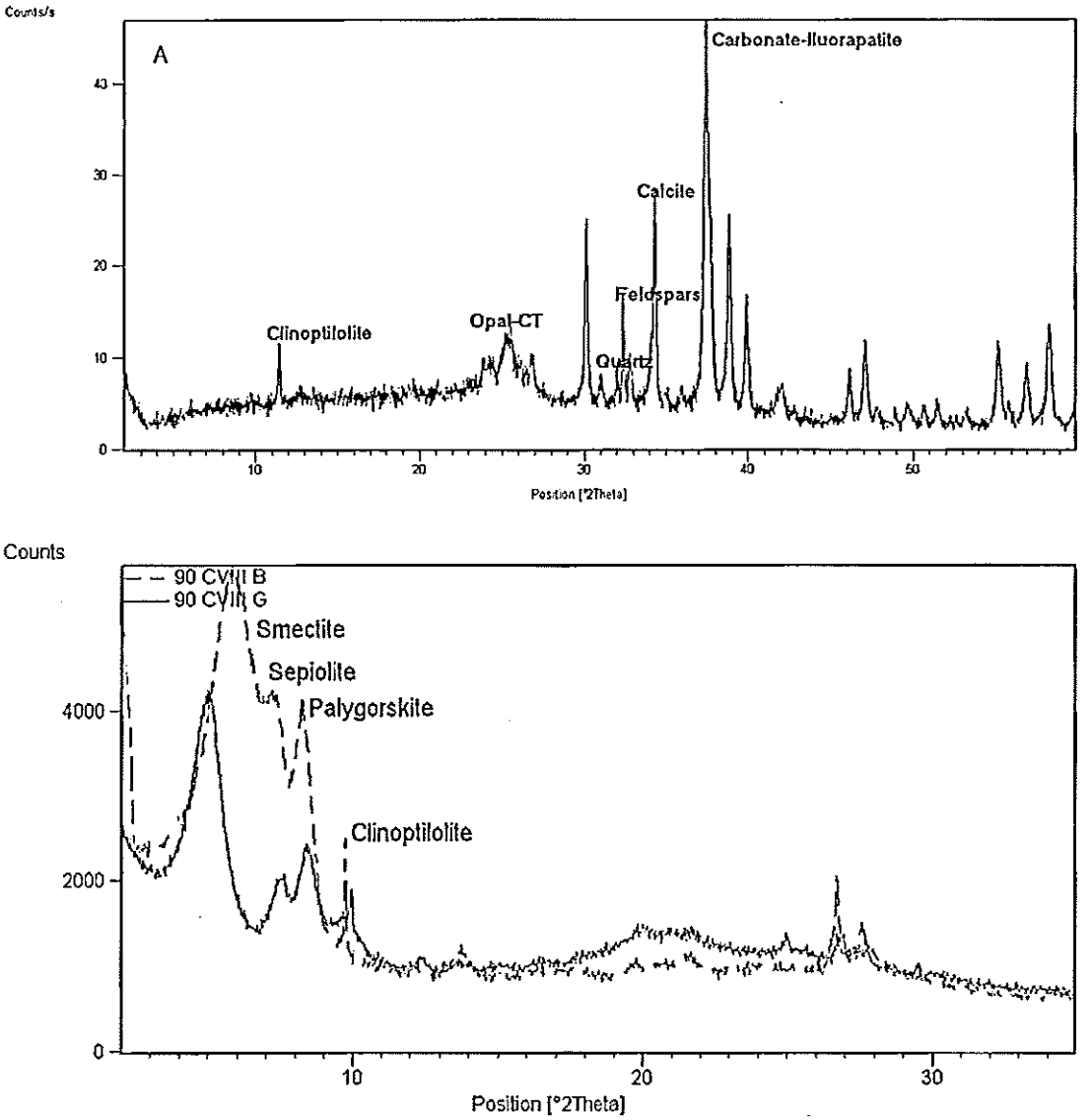

Fig. 4. A: XRays Diffractometric (XRD) diagrams of powder sample 90 CVIII. B: XRD clays diagrams of sample 90 CVIII (90 CVIII B: untreated and 90 CVIII G: glycolated).

overlain by limestones and dolomites (35 m). It is attributed to the lower Eocene named Metlaoui sensu stricto member.

- The Jebs Formation dated as Late Eocene and composed by a gypsum series (90 m), is overlain by a Mio–Plio–Quaternary "continental complex", which is composed of detrital fluvio-deltaic sediments.

The Oum El Khecheb cross section includes from base to top, the Chouabine and the Metlaoui s.s members (Fig. 3). CIII and CIV do not appear.

Materials and Methods

Eighteen (18) samples were collected from the Chouabine and Metlaoui s.s members correlated to the nine mined layers as well as to some other phosphate occurrences of lesser importance. In addition, 2 samples were collected in the cherts for comparison. Analyses are made on whole rocks without purification. The mineralogy of these samples was first documented using optical microscopy. In addition, the mineralogical proportions were determined by X-ray diffractometry (XRD with a Pan-Analytical brand X'PERT PRO type) carried out at the Laboratory of Mineral Resources and Environment of the Faculty of Sciences of Tunis. Clay argillaceous minerals determination was based on oriented clay slides, using three preparations (untreated, glycolated and heated one hour at 550°C).

Major elements (P, Ca, Si, Al, Fe, Mg, Na, K and Ti), whole rock analyses were performed at the École des Mines de Saint-Etienne—France (ENSM-SE) by X-Ray Fluorescence (XRF). Trace elements (Cd, Zn, Cr, Cu, Ni and Sr) and rare earth elements (La, Ce, Nd, Sm, Eu, Gd, Dy and Yb) were analyzed also at the ENSM-SE, by Inductively Coupled Plasma Atomic Emission Spectrometry (ICP-AES) with an Activa-Horiba Jobin Yvon Spectrometer, on a rock powder solution obtained by acid attack (nitric, hydrochloric, hydrofluoric). The following trace elements (Tb, Sc, Co, Rb, Sb, Ba, Hf, Ta, Th, U, As, Mo, Zr and Cs) were analyzed by neutron activation analyses at the Laboratoire Eugene Süe, Saclay—France. The analyses of the rare earth elements were confirmed by neutron activation analysis.

Fluorine and total sulphur were determined at "Service d'Analyses des Roches et des Minéraux - CNRS-CRPG - France". Fluorine is measured with a specific electrode after adding 500 mg of powder to soda ash. Total sulphur is analyzed after calcination (1400°C), from 25 to 250 mg of powder under oxygen current (LECO Apparatus). Statistical calculations were made with Statistical 6.0 software.

Results and Discussion

Petrography of the phosphorites

Phosphatic mineralization in the studied area consists mainly of unconsolidated phosphate grains. Phosphorites may be cemented by calcite and rarely by dolomite or silica. The phosphate fraction is quite similar to those studied elsewhere within the Gafsa Basin (Sassi, 1974; Chaabani, 1978, 1995; Belayouni, 1983; Béji Sassi, 1984, 1999; Zaïer, 1984, 1999). The petrographic observation of selected samples of phosphorites from Oum El Khecheb section has yielded the following:

- Pellets, ranging from 50 to 150 m approximately, with or without nuclei, are composed of cryptocrystalline apatite, locally enriched with scattered or organized organic matter. The arrangement and abundance of this organic matter, the nature of nucleus and the internal microporosity are at the origin of various ranges of pellets.
- Brittle coproliths, up to 1 or 2 cm, showing various forms, also consisting of cryptocrystalline apatite, with a fine silty fraction.
- Bone clasts, whose form and size relate to the intensity of the reworking that they have undergone before their immobilization; these clasts are good indicators of the depositional environment energy.
- Phosphatized bioclasts, consisting of up to 1 cm of internal moulds of gastropod and lamellibranch fragments.

Significant intraporosity is locally detected in the coproliths, pellets and other phosphatic grains. This internal microporosity increases the contact surface with the aqueous environment and eases the absorption of trace elements contained in the apatite lattice.

We note the presence of rare and free pyrite and sphalerite crystals and within the apatite pellets suggesting that these sulfides were precipitated during the grains genesis in the sedimentary basin in a zone favoring the sulphate reduction.

Silicates are also present and are mainly represented by: (i) silica, observed both as grains of microscopic quartz (some of them non-detrital) and opal–cristobalite–tridymite (opal-CT); (ii) volcanic feldspars, commonly subhedral, in places with growth zonations; and (iii) very rare glauconitic grains, arenitic in size, occasionally forming an apatitic-glauconitic mixed phase. Argillaceous matrix is characteristic of the unconsolidated phospharenites, whereas calcite constitutes both the cement and a large part of the bioclasitic allochems or lithoclasts. Dolomite is also present as cement in the Upper Phosphorite zone, but is present as scattered euhedral micro-rhombs with a dark nucleus or with zonations. Round and flat decimetric nodular limy structures, commonly observed within the phosphate layers, are constituted mainly of micritic fine debris: benthic Foraminifera, Ostracods, phosphatic grains, fish teeth, shell-clasts, phosphatized bioclasts, sparsely distributed glauconitic grains, angular quartz and/or feldspar crystals, and scarce dolomitic crystals.

Detrital terrigenous inputs sensu stricto do not constitute individualized deposits in the phosphatic series, but it is possible sometimes to find among allochems, a minor fraction formed by detrital rounded quartz, their different form distinguish them from the quartz of volcanic origin.

Mineralogy

The XRD powder diagrams of various rocks confirm the mineralogical petrographic study. We recognized carbonate fluorapatite (CFA) (2.77 Å), dolomite (2.89 Å), calcite (3.034 Å), quartz (3.34 Å) and opal-CT (4.26 Å and 4.07 Å). Moreover; the patterns reveal the presence of clinoptilolite (8.97 Å) and different types of feldspars (3.10–3.22 Å). Gypsum is also present (7.56 Å) (Fig. 4A). When it is associated with phosphorites, it corresponds to a late phase linked to meteoric water circulation. It is therefore of secondary origin (Coque, 1958; Sassi, 1962). The mineralogical distribution along the profile (Fig. 5) clearly illustrates the dominance of the CFA in the phosphatic layers.

Dolomite is almost absent from the mineral-bearing layers. It characterizes the higher part of the Main Phosphatic Series (layer 29) and the Upper Phosphate, contributing thus to the reduction in the percentages of the CFA in the phosphatic series of the Upper Phosphate (layer

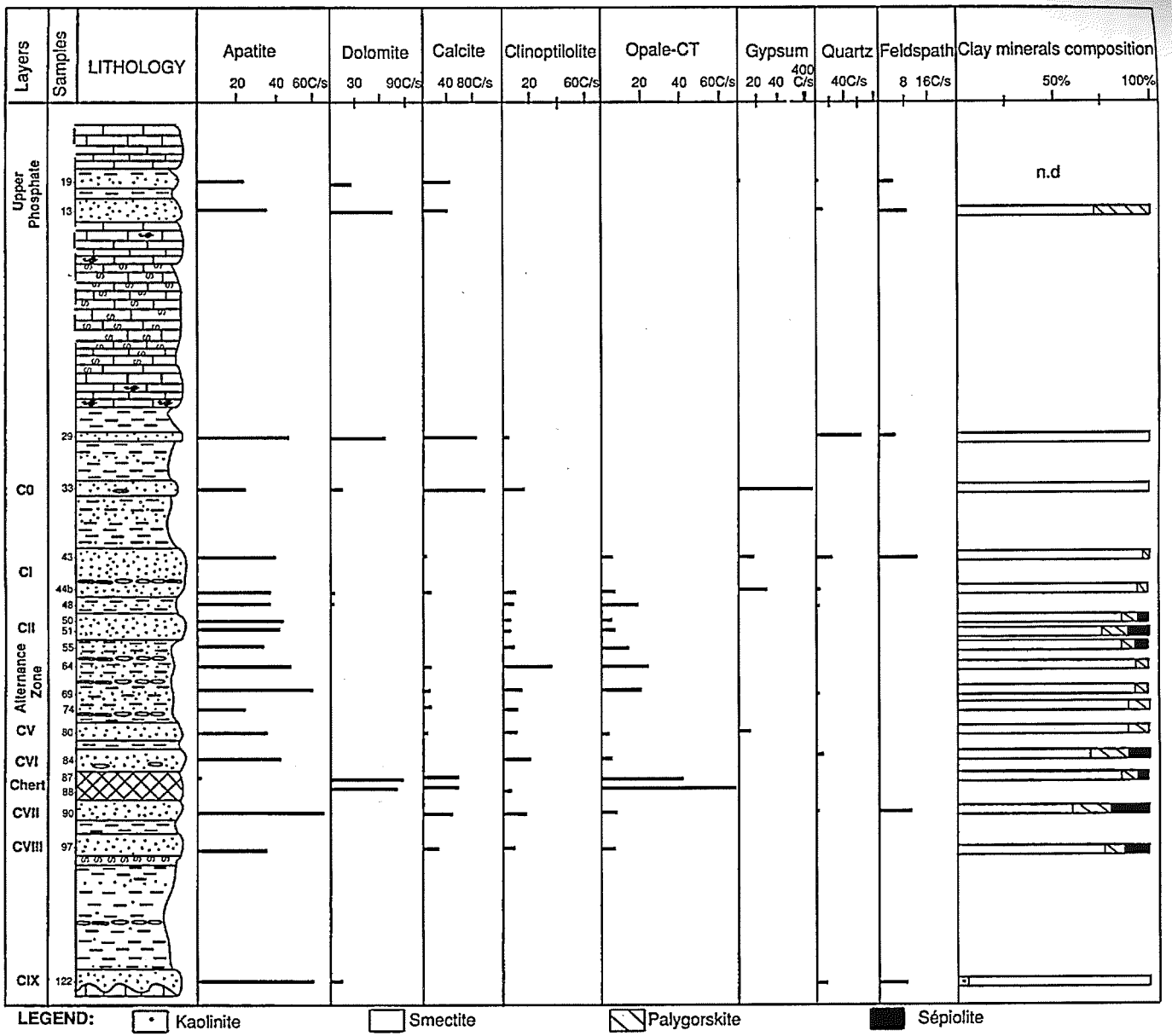

Fig. 5. Mineralogical composition in the main phosphatic layers and chert. Scale of clays minerals is in %; scales of non-clays minerals are in C/s and represent peaks length.

13). It is also present in the cherts.

Calcite, which is moderately abundant in phosphorites, characterizes some mineral-bearing layers and represents a bioclastic sedimentary fraction. It is also present in the cherts. Along the GMB profile, feldspar is sparse; grains were observed solely in the following layers: CIX, CVII, CI and in the Upper Phosphate. Quartz was recognized in several layers. The maximum abundance is recorded in layer 29 located between Upper Phosphate and C0. Opal-CT, which constitutes the main component of the cherts, is also observed in some phosphate layers.

Sassi and Jacob (1972) reported for the first time the presence of clinoptilolite in the GMB. Along the Oum El Khecheb series, this mineral is associated with the phosphate mineralization in most of the studied layers, especially within the Main Phosphatic Series, but absent in the Upper Phosphate recurrence in the higher part of the Metlaoui Formation. In addition, we observed clinoptilolite, commonly associated with opal-CT, particularly in the mineral-bearing Alternation Zone unit.

The presence of secondary gypsum is linked to the existence of the thick gypsiferous series (Jebs Formation equivalent) on top of Metlaoui Formation. Moreover, the Gafsa–Metlaoui palaeoclimate is characterized by drastic aridity, leading to a seabkha environment where gypsum crystals are exposed to a wind deflation followed by a general powdering in the area (Coque, 1958; Sassi, 1962). Later, solutions resulting from rainwater dissolution are transported and variably deposited.

Clay mineralogy alongside the profile is illustrated in Fig. 5. The argillaceous fraction is mainly made up of smectite (up to 100% in the layer C0 (33) and the upper part of the principal phosphatic series, sample 29), then by palygorskite, sepiolite, and kaolinite (Fig. 4B). Kaolinite is recognized only at the bottom of the main phosphatic series, with little content, in the layer CIX (5%). Magnesian clays (palygorskite locally accompanied by sepiolite) characterize the mineral bearing horizons CVIII, CVII, CVI and CII. The smectite is inherited from the upper Cretaceous and the Lower Paleocene, where it is very abundant, but the palygorskite and the sepiolite are neoformed from the smectite.

Chemical composition

Major and trace element compositions Table 1 presents the major and trace element compositions of selected whole rock samples. The statistical tool treatments of matrix of correlation are given in Table 2.

Factor analyses reduce a large number of initial variables in a small number of resultant variables called factors (Table 3 and Fig. 6). The factors include elements strongly covariant between them. Factor analyses determine for each variable its degree of relationship with each factor represented by a factorial axe. These axes may be drawn by couple defining factorial plans. This representation allows to visualize the projection of the analyzed elements on a plan giving a points cloud.

The whole points cloud obtained can be divided into several areas. The observed associations reflect the different minerals structures: francolite (P_2O_5, F, CaO, Sr, REE, Cr, Ba, Zr, Th, and U), clay minerals and silicates (Al_2O_3, K_2O, Fe_2O_3, MgO, TiO_2, Cs, Co, Rb, Sb, Mo, Ta, Hf, Cu, and Sc), sulphides and organic matter (Zn, Cd, Ni, Cu), free silica (opal-CT), and iron oxides (Fe_2O_3, Ni) (Table 3 and Fig. 6).

Some elements belong to different mineral structures at the same time, such SiO_2, MgO, CaO, Fe_2O_3, Na_2O, and SO_3. But, each one of these minerals has their associated elements. Indeed, except the free silica, Si exists in the phyllosilicates, the zeolite and the rare feldspars. Ca is common in carbonates (calcite and dolomite), the CFA and the gypsum. Na is associated with different silicates, CFA and Mg. This latter is shared between dolomite and magnesian clays. All these elements belonging to several minerals, explain the average values of the factor scores of Table 3.

a) Major elements

The average and standard deviation (σ) of element abundances are given in Table 1. The major element compositions are illustrated in Fig. 7. All phosphatic levels (C: I to IX) are economically significant with P_2O_5 values range between 23 and 29%. These ore grades are actually mined in the GMB. The Alternation Zone unit (Fig. 3) shows thinnest phosphatic levels with P_2O_5 contents ranging from 20.4% (layer 74) to 24.8% (layer 55). These contents decrease in the upper part of the series (C0) and the Upper Phosphorites.

The mean concentration of CaO in the mineral-bearing layers is about 38%. It correlates strongly with P_2O_5 ($r = 0.90$) as shown in Table 2. Indeed, CaO/P_2O_5 ratio in the GMB mineralized layers is close to 1.55. This value is characteristic of the CFA and obtained from purified samples measured from whole rock and purified minerals (Sassi, 1974; Slansky, 1980; McClellan and Van Kauwerbergh, 1990; Chaabani, 1995; Zaïer, 1995; Béji Sassi, 1999). Upper values indicate carbonate minerals (calcite and dolomite) associated to CFA. Samples of this study are not purified. CaO/P_2O_5 ratio is up to 1.65 if we exclude the Upper Phosphates (Table 1); but some values are close to 1.60 or less.

As Mg cannot enter in the CFA lattice, its percentage does not exhibit any high values in the P_2O_5-rich stratigraphic levels, as the element is present only in carbonates and silicates. Magnesium is located within Mg-silicates, in accord with the rough negative correlation observed on the variation curves of MgO and P_2O_5 ($r = -0.79$). We used a formula to assign the respective parts of CaO in the dolomite and in the apatite lattices.

Table 1. Major (%) and trace elements (ppm) and rare earth elements (ppm) in the main phosphatic layers, Chert and the UCC (Taylor and McLennan, 1985)

Samples	Uph 19	Uph 13	29 29	C0 33	CI 43	CI 44b	48 48	CII 50	CII 51	Alz 55	Alz 64
LOI	30.12	20.61	17.62	20.65	10.67	13.76	11.13	12.21	11.63	11.68	12.37
SiO_2	4.93	9.53	16.11	7.95	14.47	11.07	24.34	5.35	11.05	16.69	20.60
TiO_2	0.03	0.15	0.09	0.08	0.11	0.09	0.04	0.04	0.05	0.06	0.07
Al_2O_3	0.22	1.33	1.66	1.39	2.79	2.00	0.83	0.74	0.95	1.40	1.49
Fe_2O_3	0.25	0.55	1.77	4.37	1.10	0.91	0.44	0.44	0.55	0.72	0.64
MgO	3.27	4.49	1.83	1.02	0.66	0.95	0.55	0.67	0.70	0.86	0.75
CaO	40.50	40.59	39.37	38.22	40.78	40.66	36.03	45.92	44.35	39.15	36.96
Na_2O	0.64	0.67	0.54	0.38	0.96	0.91	0.79	1.20	1.04	0.98	0.93
K_2O	0.00	0.25	0.40	0.24	0.39	0.25	0.15	0.06	0.14	0.16	0.22
P_2O_5	16.20	18.26	17.97	12.16	24.04	23.73	22.58	28.81	27.80	24.77	23.17
SO_3	3.08	2.33	1.83	11.13	3.53	2.50	2.30	3.08	3.18	2.45	2.20
F	2.14	2.33	2.17	1.50	3.16	2.60	2.40	3.26	3.05	2.83	2.50
Total	101.38	101.09	101.36	99.09	102.66	99.43	101.58	101.78	104.49	101.75	101.90
F=O	0.90	0.98	0.91	0.63	1.33	1.09	1.01	1.37	1.28	1.19	1.05
Total	100.48	100.11	100.45	98.46	101.33	98.34	100.57	100.41	103.21	100.56	100.85
CaO/P_2O_5	2.50	2.22	2.19	3.14	1.70	1.71	1.60	1.59	1.60	1.58	1.59
SiO_2/Al_2O_3	22.41	7.17	9.70	5.72	5.19	5.54	29.33	7.23	11.63	11.92	13.83
Cd	32.29	40.53	30.98	149.31	41.00	61.24	59.68	87.83	49.80	15.34	15.03
Zn	151	205.24	574	592.84	416.54	433.45	400	621	416.80	133.81	130.99
Cr	119.18	156.91	268.62	206.39	244.25	351.51	290.73	462.01	454.10	168.79	168.23
Cu	17.60	27.31	35.53	33.59	16.40	20.90	9.60	16.21	15.82	14.77	7.30
Ni	11.70	13.87	38.34	114.40	13.78	26.09	27.54	18.13	13.95	9.75	7.25
Sr	1241	1171	1405	1048	1916	1652	1541	1995	1902	1811	1661
Sc	1.10	2.50	2.90	2.70	3.70	4.60	2.70	3.30	3.20	2.90	3.50
Co	0.20	0.46	0.82	1.43	0.82	1.92	2.01	0.78	0.67	1.65	0.69
Rb	2.20	6.40	9.00	7.30	5.70	8.80	4.60	4.60	4.20	6.90	6.40
Sb	0.53	0.88	0.71	0.65	0.88	0.79	0.47	0.28	0.24	0.22	0.20
Cs	0.12	0.24	0.37	0.40	0.32	0.60	0.32	0.31	0.32	0.49	0.44
Ba	45.9	82.0	88.0	51.6	73.0	64.0	52.3	58.0	55.8	50.0	45.1
Hf	0.64	1.91	1.25	0.61	0.67	0.52	0.29	0.40	0.35	0.36	0.49
Ta	0.07	0.74	0.26	0.22	0.24	0.26	0.10	0.08	0.09	0.14	0.15
Th	1.13	2.66	8.57	5.83	16.31	9.89	4.12	10.08	11.37	7.99	6.88
U	26.2	27.1	19.5	15.2	29.8	26.2	21.1	28.0	24.6	22.6	13.2
As	4.79	16.05	14.80	14.07	3.08	4.37	3.70	1.77	1.77	2.39	2.86
Mo	23.40	22.10	25.40	19.60	9.35	22.50	16.80	12.23	9.06	9.11	5.26
Zr	77	135	98	52	96	81	61	78	77	63	56
Total	1775	1926	2651	2349	2931	2770	2546	3448	3092	2376	2195
Zn/Cd	4.68	5.06	18.53	3.97	10.16	7.08	6.70	7.07	8.37	8.72	8.72
Zr/Hf	120.31	70.68	78.40	85.25	143.28	155.77	210.34	195.00	220.00	175.00	114.29
La	25.2	45.5	61.1	39.7	110.0	73.6	58.5	88.9	93.2	74.3	73.1
Ce	21.7	52.1	100.4	64.0	200.0	106.4	69.1	136.8	157.0	132.4	134.6
Nd	18.2	32.6	61.0	35.4	111.1	63.6	48.1	80.7	90.8	72.5	65.8
Sm	2.90	5.39	11.47	7.06	21.22	11.90	8.11	15.12	16.90	13.59	12.66
Eu	0.99	1.97	3.07	1.99	5.66	3.08	2.13	4.32	4.21	3.65	3.43
Gd	4.39	8.00	14.57	9.00	22.65	14.78	10.26	16.74	18.92	15.46	13.77
Tb	0.57	1.01	1.54	1.02	2.72	1.69	1.30	2.11	2.26	1.78	1.68
Dy	4.26	7.10	10.41	6.59	17.51	12.15	9.20	14.54	15.67	12.84	11.30
Yb	2.58	4.36	5.04	3.81	8.52	6.81	5.63	8.16	8.00	6.22	6.12
Total	80.79	158.03	268.60	168.57	499.38	294.01	212.33	367.39	406.96	332.74	322.46
La/Yb	9.77	10.44	12.12	10.42	12.91	10.81	10.39	10.89	11.65	11.95	11.94
La_N/Yb_N	0.72	0.77	0.89	0.76	0.95	0.79	0.76	0.80	0.85	0.88	0.88
Dy_N/Sm_N	1.89	1.69	1.17	1.20	1.06	1.31	1.46	1.24	1.19	1.21	1.15
Ce/Ce*	0.45	0.61	0.70	0.74	0.77	0.68	0.57	0.70	0.73	0.77	0.84
Eu/Eu*	1.25	1.36	1.09	1.15	1.20	1.07	1.08	1.26	1.10	1.17	1.21
Tb/Tb*	0.74	0.76	0.71	0.75	0.78	0.72	0.76	0.77	0.75	0.72	0.77
Sm/Sm*	0.71	0.69	0.87	0.87	0.88	0.89	0.84	0.84	0.91	0.87	0.88

Table 1. (continued)

Samples	Alz 69	Alz 74	CV 80	CVI 84	Ch 87	Ch 88	CVII 90	CVIII 97	CIX 122	Average	σ	UCC
LOI	11.29	14.80	12.36	12.26	19.26	19.82	14.36	13.01	11.36	15.05	4.91	—
SiO_2	19.13	17.88	7.96	6.92	53.50	56.43	4.56	12.96	8.29	16.49	14.29	66
TiO_2	0.05	0.15	0.06	0.05	0.20	0.20	0.06	0.06	0.10	0.09	0.05	0.41
Al_2O_3	0.97	3.47	1.18	1.00	4.24	4.27	0.96	1.02	2.49	1.72	1.15	15.20
Fe_2O_3	0.50	1.59	0.70	0.61	1.70	1.65	0.50	0.52	1.79	1.07	0.93	4.50
MgO	0.64	1.53	0.70	0.83	4.14	4.28	1.23	0.74	1.32	1.56	1.33	2.20
CaO	40.15	34.87	43.34	45.28	13.02	9.41	46.58	43.37	42.03	38.03	9.72	4.20
Na_2O	1.16	0.68	1.16	1.16	1.37	1.37	1.08	1.14	1.24	0.97	0.28	3.90
K_2O	1.15	0.40	0.12	0.08	0.53	0.44	0.25	0.16	0.69	0.30	0.26	3.40
P_2O_5	24.57	20.39	25.91	28.12	1.40	0.87	26.74	25.31	26.09	20.94	8.01	0.32
SO_3	2.50	2.00	4.13	2.83	0.20	0.20	3.15	2.60	3.50	2.94	2.16	—
F	2.60	2.40	2.94	3.11	0.00	0.00	3.13	2.83	3.14	2.40	0.93	—
Total	104.71	100.16	100.56	102.25	99.56	98.94	102.60	103.72	102.04	—	—	—
F = O	1.09	1.01	1.23	1.31	0.00	0.00	1.31	1.19	1.32	—	—	—
Total	103.62	99.15	99.33	100.94	99.56	98.94	101.29	102.53	100.72	—	—	—
CaO/P_2O_5	1.63	1.71	1.67	1.61	9.25	10.84	1.74	1.71	1.61	—	—	13.13
SiO_2/Al_2O_3	19.72	5.15	6.75	6.92	12.62	13.22	4.75	12.71	3.33	—	—	4.34
Cd	9.46	15.17	24.18	33.18	70.87	46.04	57.69	20.36	13.71	43.68	32.85	0.10
Zn	124.22	58.84	216.94	227.70	809.26	543	434.78	152.46	115.18	337.91	214.14	71
Cr	228.38	190.82	241.77	179.78	161.85	159.00	185.58	156.95	127.64	226.12	97.69	83
Cu	8.75	12.25	9.71	13.10	30.40	29.00	13.85	13.04	15.86	18.05	8.54	25
Ni	7.53	17.11	13.42	14.44	43.09	57.00	20.02	16.70	20.07	25.21	24.50	44
Sr	1637	1540	1894	1915	234	196	1839	1680	1750	1501.35	511.76	350
Sc	3.00	4.80	3.80	3.00	3.60	3.49	2.70	2.50	4.20	3.21	0.82	13.60
Co	0.55	3.50	1.30	1.17	5.40	5.25	0.49	0.70	4.00	1.69	1.58	17
Rb	5.00	13.60	5.70	3.90	15.00	14.60	4.20	4.50	13.30	7.30	3.87	112
Sb	0.12	0.36	0.27	0.33	0.80	0.71	0.26	0.26	0.96	0.50	0.27	0.20
Cs	0.36	0.96	0.37	0.26	1.20	1.07	0.30	0.28	0.90	0.48	0.30	4.60
Ba	40.6	53.3	63.5	67.1	33.0	26.8	64.5	56.4	78.0	57.45	15.67	550
Hf	0.42	0.97	0.48	0.45	0.95	0.88	0.46	0.33	0.56	0.65	0.39	5.80
Ta	0.12	0.40	0.13	0.11	0.60	0.50	0.16	0.12	0.23	0.24	0.19	1.00
Th	4.68	5.67	8.24	7.46	2.80	2.21	3.38	2.80	18.42	7.02	4.59	10.70
U	17.6	13.1	25.4	37.4	3.6	3.2	40.5	31.4	51.9	23.88	11.67	2.80
As	7.34	8.18	2.51	2.79	8.20	7.20	1.56	1.90	12.00	6.07	4.75	1.50
Mo	4.05	7.51	8.66	14.97	13.50	13.30	16.52	8.67	36.40	14.92	8.06	1.50
Zr	63	80	80	95	43	39	114	79	123	79.50	25.34	190
Total	2231	2100	2680	2701	1568	1236	2890	2325	2508	—	—	1484
Zn/Cd	13.13	3.88	8.97	6.86	11.42	11.79	7.54	7.49	8.40	—	—	710
Zr/Hf	150.00	82.47	166.67	211.11	45.26	44.32	247.83	239.39	219.64	—	—	32.76
La	65.4	58.3	77.8	70.3	9.8	9.3	54.1	41.8	139.8	63.49	31.51	30
Ce	97.4	102.7	119.4	110.8	16.1	15.8	60.5	49.2	292.0	101.92	66.15	64
Nd	54.1	48.2	68.3	62.6	8.1	7.9	38.5	31.8	159.4	57.94	35.65	26
Sm	9.87	9.47	13.14	10.96	1.35	1.30	5.31	4.02	32.20	10.70	7.30	4.50
Eu	2.78	2.58	3.65	3.32	0.42	0.43	2.07	1.65	8.57	3.00	1.86	0.88
Gd	10.80	12.76	15.58	13.47	2.00	1.90	9.98	7.35	34.85	12.86	7.44	3.80
Tb	1.43	1.30	1.89	1.69	0.22	0.21	1.19	0.89	4.06	1.53	0.87	0.64
Dy	9.97	9.28	13.13	11.82	1.70	1.50	9.15	6.54	24.00	10.43	5.32	3.50
Yb	5.91	5.28	7.62	6.69	0.79	0.76	6.53	4.81	10.80	5.72	2.49	2.20
Total	257.66	249.87	320.51	291.65	40.50	39.10	187.33	148.06	705.68	—	—	135.52
La/Yb	11.07	11.04	10.21	10.51	12.43	12.24	8.28	8.69	12.94	—	—	13.64
La_N/Yb_N	0.81	0.81	0.75	0.77	0.91	0.90	0.61	0.64	0.95	—	—	—
Dy_N/Sm_N	1.30	1.26	1.28	1.39	1.62	1.48	2.22	2.09	0.96	—	—	—
Ce/Ce*	0.72	0.85	0.71	0.73	0.79	0.81	0.60	0.60	0.81	—	—	—
Eu/Eu*	1.25	1.07	1.18	1.26	1.16	1.24	1.24	1.33	1.19	—	—	—
Tb/Tb*	0.79	0.68	0.75	0.76	0.68	0.71	0.71	0.73	0.79	—	—	—
Sm/Sm*	0.84	0.88	0.86	0.79	0.76	0.73	0.62	0.58	0.90	—	—	—

Table 2. Matrix correlations between trace elements and major elements in phosphorites of Oum El Khecheb profile. Level of significance at 99% is 0.54 with N = 20

	LOI	SiO_2	TiO_2	Al_2O_3	Fe_2O_3	MgO	CaO	Na_2O	K_2O	P_2O_5	SO_3	F	Cd	Zn	Cr	Cu	Ni	Sr	Sc
LOI	1.00																		
SiO_2	0.14	1.00																	
TiO_2	0.27	0.73	1.00																
Al_2O_3	0.06	0.76	0.92	1.00															
Fe_2O_3	0.25	0.18	0.38	0.41	1.00														
MgO	0.75	0.55	0.72	0.48	0.11	1.00													
CaO	−0.34	−0.96	−0.80	−0.80	−0.32	−0.67	1.00												
Na_2O	−0.31	0.28	0.34	0.48	−0.27	0.07	−0.23	1.00											
K_2O	−0.18	0.34	0.34	0.40	0.20	0.08	−0.28	−0.20	1.00										
P_2O_5	−0.65	−0.79	−0.75	−0.66	−0.50	−0.79	0.90	0.01	−0.18	1.00									
SO_3	0.09	−0.52	−0.35	−0.36	0.62	−0.37	0.40	−0.47	−0.17	0.14	1.00								
F	−0.57	−0.85	−0.73	−0.65	−0.46	−0.74	0.94	0.03	−0.21	0.98	0.19	1.00							
Cd	0.27	0.00	0.05	−0.01	0.60	0.05	−0.11	−0.22	−0.25	−0.31	0.62	−0.31	1.00						
Zn	0.18	0.42	0.32	0.32	0.39	0.25	−0.43	0.12	−0.06	−0.50	0.06	−0.51	0.73	1.00					
Cr	−0.39	−0.22	−0.33	−0.26	−0.17	−0.43	0.30	0.02	−0.20	0.40	0.07	0.32	0.33	0.40	1.00				
Cu	0.58	0.34	0.56	0.39	0.64	0.61	−0.46	−0.18	0.05	−0.70	0.14	−0.64	0.53	0.66	−0.06	1.00			
Ni	0.38	0.27	0.31	0.28	0.90	0.20	−0.40	−0.32	0.02	−0.61	0.59	−0.59	0.79	0.59	−0.06	0.71	1.00		
Sr	−0.64	−0.80	−0.76	−0.63	−0.44	−0.83	0.90	0.04	−0.22	0.98	0.20	0.98	−0.29	−0.47	0.39	−0.68	−0.57	1.00	
Sc	−0.53	0.21	0.43	0.61	0.20	−0.21	−0.18	0.42	0.31	0.07	−0.16	0.02	−0.12	0.03	0.22	−0.10	−0.04	0.09	1.00
Co	0.08	0.77	0.76	0.87	0.39	0.45	−0.81	0.41	0.33	−0.66	−0.33	−0.68	0.05	0.29	−0.26	0.31	0.33	−0.66	0.52
Rb	0.09	0.67	0.85	0.91	0.50	0.47	−0.73	0.29	0.45	−0.62	−0.29	−0.63	−0.02	0.25	−0.27	0.45	0.34	0.62	0.63
Sb	0.35	0.23	0.60	0.52	0.44	0.53	−0.35	0.15	0.17	−0.48	0.01	−0.38	0.24	0.35	−0.20	0.66	0.37	−0.47	0.18
Cs	0.03	0.74	0.80	0.91	0.40	0.41	−0.78	0.38	0.43	−0.60	−0.35	−0.64	−0.02	0.25	−0.24	0.29	0.27	−0.61	0.63
Ba	−0.20	−0.64	−0.19	−0.28	−0.04	−0.21	0.64	−0.01	−0.13	0.51	0.16	0.60	−0.12	−0.13	0.13	0.10	−0.20	0.52	0.07
Hf	0.50	0.20	0.65	0.36	0.20	0.75	−0.30	−0.12	0.13	−0.47	−0.20	−0.38	−0.01	0.12	−0.28	0.63	0.13	−0.48	−0.01
Ta	0.37	0.53	0.91	0.68	0.27	0.81	−0.61	0.13	0.24	−0.66	−0.30	−0.62	0.08	0.25	−0.33	0.59	0.23	−0.69	0.23
Th	−0.57	−0.33	−0.14	0.08	0.11	−0.49	0.37	0.34	0.13	0.48	0.18	0.52	−0.10	−0.04	0.35	−0.14	−0.16	0.53	0.52
U	−0.31	−0.73	−0.49	−0.46	−0.28	−0.38	0.74	0.17	−0.14	0.70	0.18	0.77	−0.20	−0.36	0.00	−0.35	−0.38	0.68	−0.08
As	0.44	0.11	0.48	0.28	0.62	0.50	−0.23	−0.47	0.40	−0.46	0.21	−0.39	0.19	0.13	−0.30	0.70	0.49	−0.48	0.00
Mo	0.37	−0.21	0.08	−0.01	0.29	0.30	0.08	−0.13	−0.01	−0.12	0.15	−0.04	0.18	0.13	−0.17	0.47	0.26	−0.14	−0.10
Zr	−0.09	−0.63	−0.12	−0.27	−0.24	−0.01	0.61	0.08	−0.04	0.50	0.01	0.60	−0.26	−0.31	−0.06	−0.05	−0.39	0.47	−0.02
La	−0.69	−0.54	−0.38	−0.20	−0.15	−0.64	0.61	0.22	0.10	0.75	0.16	0.77	−0.26	−0.31	0.35	−0.44	−0.40	0.77	0.42
Ce	−0.63	−0.40	−0.23	−0.03	−0.01	−0.54	0.45	0.27	0.19	0.60	0.14	0.62	−0.28	−0.29	0.23	−0.34	−0.31	0.63	0.48
Nd	−0.63	−0.44	−0.29	−0.10	−0.05	−0.56	0.50	0.26	0.15	0.64	0.15	0.66	−0.25	−0.26	0.28	−0.34	−0.32	0.66	0.42
Sm	−0.59	−0.40	−0.24	−0.04	0.01	−0.52	0.45	0.24	0.17	0.58	0.16	0.61	−0.23	−0.24	0.26	−0.30	−0.28	0.61	0.46
Eu	−0.59	−0.46	−0.26	−0.08	−0.02	−0.52	0.50	0.25	0.16	0.62	0.17	0.65	−0.25	−0.28	0.22	−0.32	−0.31	0.64	0.42
Gd	−0.60	−0.47	−0.27	−0.08	0.00	−0.55	0.52	0.24	0.14	0.64	0.17	0.66	−0.24	−0.27	0.25	−0.30	−0.29	0.66	0.45
Tb	−0.62	−0.49	−0.31	−0.13	−0.06	−0.57	0.54	0.24	0.13	0.67	0.17	0.69	−0.24	−0.28	0.27	−0.35	−0.33	0.68	0.42
Dy	−0.67	−0.54	−0.38	−0.20	−0.12	−0.63	0.60	0.23	0.08	0.74	0.16	0.76	−0.25	−0.29	0.34	−0.41	−0.38	0.76	0.41
Yb	−0.73	−0.65	−0.50	−0.35	−0.24	−0.73	0.74	0.19	0.00	0.87	0.20	0.87	−0.23	−0.33	0.40	−0.53	−0.44	0.87	0.36

	Co	Rb	Sb	Cs	Ba	Hf	Ta	Th	U	As	Mo	Zr	La	Ce	Nd	Sm	Eu	Gd	Tb	Dy	Yb
LOI																					
SiO_2																					
TiO_2																					
Al_2O_3																					
Fe_2O_3																					
MgO																					
CaO																					
Na_2O																					
K_2O																					
P_2O_5																					
SO_3																					
F																					
Cd																					
Zn																					
Cr																					
Cu																					
Ni																					
Sr																					
Sc																					
Co	1.00																				
Rb	0.91	1.00																			
Sb	0.43	0.52	1.00																		
Cs	0.96	0.96	0.38	1.00																	
Ba	−0.41	−0.20	0.33	−0.40	1.00																
Hf	0.15	0.38	0.58	0.19	0.33	1.00															
Ta	0.53	0.66	0.62	0.56	0.00	0.85	1.00														
Th	−0.01	0.09	0.26	0.04	0.51	−0.22	−0.25	1.00													
U	−0.38	−0.39	0.04	−0.42	0.67	−0.24	−0.39	0.50	1.00												
As	0.24	0.47	0.63	0.25	0.30	0.76	0.62	−0.04	−0.15	1.00											
Mo	0.16	0.21	0.70	0.07	0.51	0.32	0.18	0.23	0.46	0.57	1.00										
Zr	−0.36	−0.20	0.28	−0.34	0.87	0.37	0.11	0.35	0.79	0.24	0.50	1.00									
La	−0.23	−0.15	0.00	−0.18	0.56	−0.32	−0.41	0.92	0.65	−0.16	0.14	0.48	1.00								
Ce	−0.06	0.03	0.10	0.00	0.49	−0.26	−0.31	0.95	0.57	−0.06	0.18	0.41	0.97	1.00							
Nd	−0.11	−0.03	0.11	−0.07	0.53	−0.28	−0.35	0.95	0.63	−0.08	0.23	0.44	0.98	0.99	1.00						
Sm	−0.05	0.03	0.15	−0.01	0.51	−0.25	−0.31	0.96	0.58	−0.03	0.25	0.41	0.97	0.99	1.00	1.00					
Eu	−0.10	−0.01	0.13	−0.05	0.55	−0.24	−0.32	0.94	0.65	−0.04	0.26	0.48	0.97	0.99	0.99	0.99	1.00				
Gd	−0.09	0.01	0.14	−0.04	0.58	−0.24	−0.33	0.95	0.65	−0.03	0.28	0.49	0.98	0.99	0.99	0.99	0.99	1.00			
Tb	−0.13	−0.06	0.10	−0.10	0.56	−0.28	−0.36	0.94	0.67	−0.07	0.25	0.49	0.99	0.99	1.00	0.99	1.00	0.99	1.00		
Dy	−0.20	−0.13	0.02	−0.16	0.57	−0.32	−0.41	0.93	0.67	−0.15	0.18	0.49	1.00	0.97	0.99	0.97	0.98	0.98	0.99	1.00	
Yb	−0.35	−0.29	−0.14	−0.31	0.59	−0.39	−0.50	0.83	0.73	−0.27	0.09	0.53	0.97	0.89	0.92	0.89	0.91	0.92	0.93	0.96	1.00

Table 3. Factor Weight (without rotation) - Extraction: principal components (marked weight)

	Factor 1	Factor 2	Factor 3
LOI	0.65	0.20	–0.50
SiO_2	0.77	–0.30	0.48
TiO_2	0.70	–0.62	0.08
Al_2O_3	0.56	–0.72	0.30
Fe_2O_3	0.36	–0.44	–0.44
MgO	0.78	–0.17	–0.19
CaO	–0.86	0.33	–0.33
Na_2O	–0.03	–0.21	0.72
K_2O	0.11	–0.47	0.23
P_2O_5	–0.95	0.23	0.06
SO_3	–0.21	0.10	–0.59
F	–0.96	0.19	–0.06
Cd	0.29	0.05	–0.47
Zn	0.45	–0.17	–0.17
Cr	–0.36	0.07	0.06
Cu	0.62	–0.32	–0.58
Ni	0.53	–0.17	–0.45
Sr	–0.96	0.21	0.04
Sc	–0.14	–0.71	0.39
Co	0.55	–0.66	0.34
Rb	0.51	–0.79	0.18
Sb	0.29	–0.67	–0.49
Cs	0.51	–0.70	0.39
Ba	–0.57	–0.24	–0.59
Hf	0.47	–0.30	–0.48
Ta	0.66	–0.47	–0.16
Th	–0.71	–0.63	–0.03
U	–0.76	–0.06	–0.28
As	0.37	–0.46	–0.64
Mo	–0.03	–0.40	–0.67
Zr	–0.52	–0.19	–0.49
La	–0.90	–0.41	0.03
Ce	–0.80	–0.57	0.06
Nd	–0.83	–0.53	0.01
Sm	–0.79	–0.58	0.01
Eu	–0.82	–0.55	–0.02
Gd	–0.82	–0.55	–0.04
Tb	–0.85	–0.51	–0.02
Dy	–0.89	–0.43	0.01
Yb	–0.96	–0.25	0.02
Var. Exp	17.10	7.84	5.12
Prp. Tot	0.43	0.20	0.13

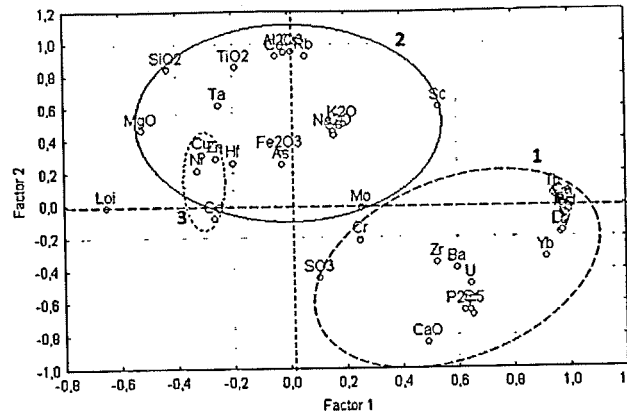

Fig. 6. Factor weight F1 versus F2. 1: CFA group, 2: Silicates group and 3: sulphides and organic matter group.

[CaO – (1.3*P_2O_5)] corresponds to the calcium in the dolomite lattice. CaO is the total analyzed calcium and (1.3*P_2O_5) corresponds to the calcium in a theoretical apatite lattice $Ca_5(PO_4)_3F$ in which, 5 CaO is equivalent to 1.5 P_2O_5. In MgO versus CaO – (1.3*P_2O_5) (Fig. 8A), MgO appears crudely related to the excess of CaO. The maximum concentration is recorded in the Upper Phosphates (4.5%) and MgO-content appears to indicate both dolomite and silicate fractions.

The fluorine-content obtained from whole rock, ranges from 1.5% in C0 layer to 3.26% in CII layer. Fluorine correlates well with P_2O_5 (r = 0.98). The calculated F/P_2O_5 ratio, ranging from 0.108 to 0.128 (mean 0.115), agrees with the previous values obtained from other profiles in the GMB and reported by Sassi (1974) by Chaabani (1995). It is higher than the theoretical CFA value that is about 0.089 (Altschuler *et al.*, 1958).

Because gypsum is meteoric in origin (Coque, 1958; Sassi, 1962) the SO_3/P_2O_5 ratio of the phosphatic series of the GMB is calculated only for samples whose XRD patterns are free of gypsum. This ratio value, about 0.11 (Fig. 8B), is similar to that given by Sassi (1974) for phosphorites of Sector 100 located to the East of Oum El Khecheb.

The Na_2O content along the series varies between 0.13 and 1.37%. It is positively correlated with the P_2O_5 content (Fig. 8C), suggesting that Na occurs in the apatite structure. Nevertheless, Na can be present not only in the apatite lattice but can also be linked to silicates such as clinoptilolite ($(Na,K,Ca)_{2-3}Al_3(Al,Si)_2Si_{13}O_{36}–12H_2O$) and may also be trapped between the smectites layers. The Na_2O/P_2O_5 ratio is about 0.04 and is close to that the Gafsa basin phosphorites (0.05) as was reported by Sassi (1974).

Free silica, derived from Diatom mud is mostly associated with mineralization. Values range from 4.5% (CVII) to 24.34% (layer 48), except in the chert units where SiO_2 is about 54–57% for 4.2% Al_2O_3. Allochems and cement are totally or partially silicified during diagenesis in these thin layers. Terrigenous quartz is very rare, but where present in some levels, quartz may have a subaerial volcanic origin (Clocchiatti and Sassi, 1972; Béji Sassi *et al.*, 1996; Béji Sassi, 1999). These different origins for silica explain its distribution within the mineralization as it appears in the factor analysis. Since Ti-rich minerals are not observed, we assume that TiO_2 (<1%) is mostly contained within silicates as shown by r (TiO_2–Al_2O_3) =

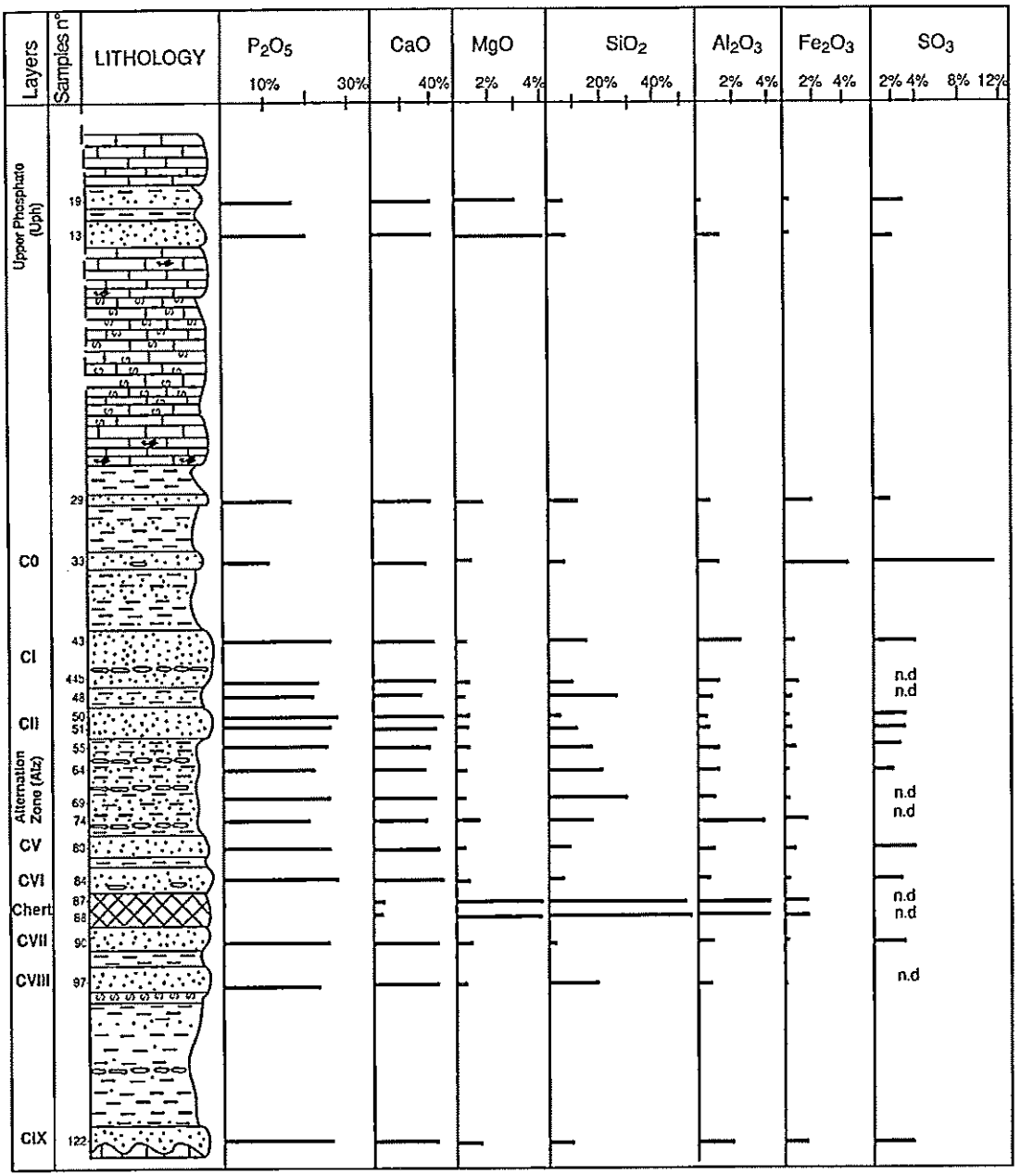

Fig. 7. Variation of the chemical composition in the main layers of phosphorites and chert of Oum El Khecheb profile.

0.92.

Aluminum is observed within silicates. The low values of Al_2O_3 (0.22–4.27%) are due to the nature of samples that are mainly phosphatic, except for samples of cherts. The same observation concerns Fe_2O_3 low content in the mineralized layers in which it ranges from 0.25% to 4.37%.

b) Trace elements

The concentration of traces elements from the analyzed rocks is presented in Table 1. Traces elements distribution along the profile does not show a regular evolution. These traces were distributed in the different mineral phases: CFA, silicates (clays, clinoptilolite, and feldspars), opal-cristobalite of the cherts, and the carbonates (calcite, dolomite).

Compared with the Upper Continental Crust composition (UCC), there is major and traces elements fractionation (Fig. 9). For values >1, the concentrations of CaO, P_2O_5, Sr, Cd, Zn, Cr, U, Mo, As and Sb are in excess relative to UCC. If values are <1, the deficit is in relation to the composition of UCC (SiO_2, TiO_2, Al_2O_3, Fe_2O_3, Zr, Ba, Rb, Sc, Co, Hf, Cs and Ta). Few elements

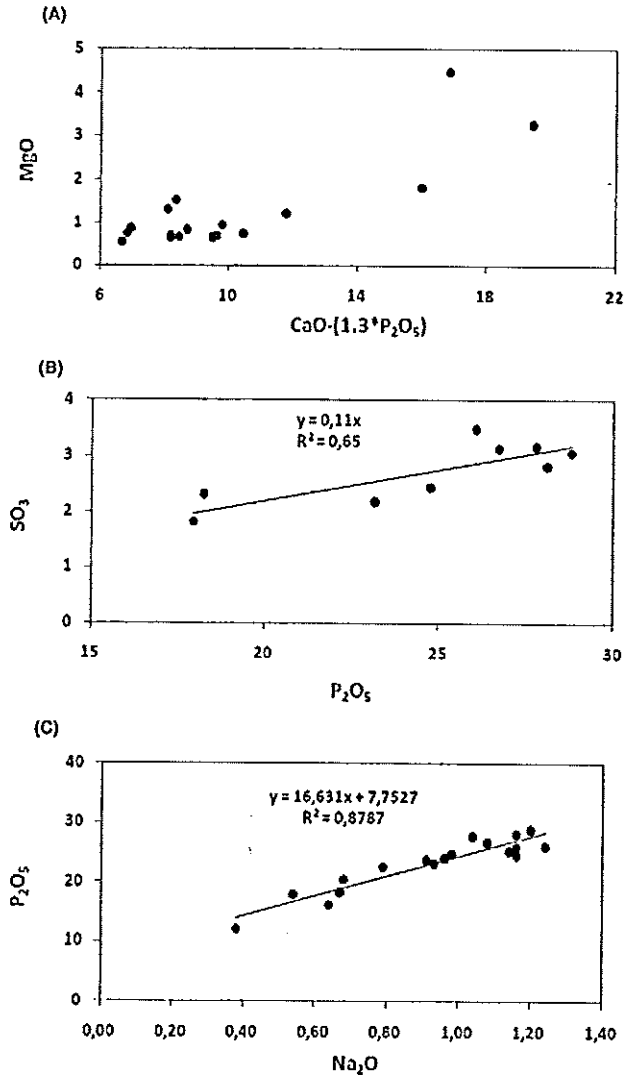

*Fig. 8. A: MgO versus CaO – (1.3*P_2O_5) diagram. B: SO_3 versus P_2O_5 diagram for phosphatic samples from Oum El Khecheb section. C: Na_2O versus P_2O_5 diagram for phosphatic samples from Oum El Khecheb Section without chert.*

have values close to UCC (MgO, Cu, Ni, Th). Elements situated above line 1, correspond mainly to the CFA. However, some of them are associated to the organic matter (Belayouni *et al.*, 1982). Despite of its low content, Cd appears to be in excess compared to the UCC values, because it rarely occurs in the crust minerals. Elements situated under line 1, corresponding to the silicates, seem to be underconcentrated relative to the UCC concentrations (constituted mainly by detrital exogen and endogen minerals).

i) Strontium, zinc, chromium, nickel, copper and cadmium

The content of the trace elements: Sr, Cd, Zn, Cr, Cu and Ni, are variable in phosphatic stratigraphic units (Table 1). Strontium is the most abundant trace element. The good Sr–P_2O_5 correlation (0.98) confirms that Sr is located in the CFA lattice.

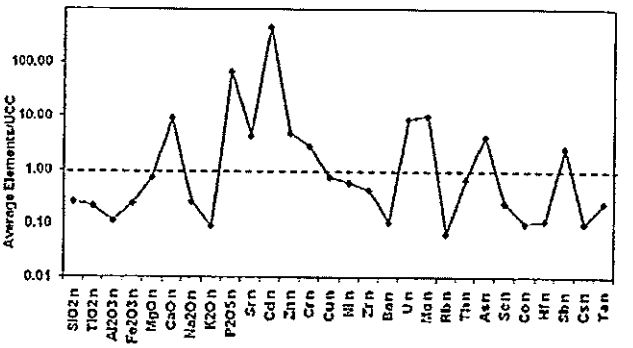

Fig. 9. UCC-normalized averages major and trace elements spectra of phosphatic samples from Oum El Khecheb profile.

The average concentration of Zn is about 338 ppm. These concentrations increase from bottom to cherts (115 to 809 ppm). The contents decrease to 227 ppm in C VI and to 59 ppm at the Alternations Zone (Fig. 3). In the upper part of the Main Phosphatic Series, the Zn-values are very high (from 417 to 620 ppm). In the Upper Phosphates (Fig. 3), Zn concentrations decrease to 150–200 ppm.

The element also present is the Cr with an average concentration of about 226 ppm. From bottom to the top of the Alternations Zone (Fig. 3), Cr content increases from: 127 to 169 ppm. From the CII bottom, there is a sharp increase (460 ppm) followed by a decrease to 270 ppm to the top of the Main Phosphatic Series. Upper Phosphates are as poor as the series bottom (120 ppm). The average concentration of Ni is 27 ppm. Ni correlates with Fe ($r = 0.9$). The average Cu content is 18 ppm.

Cadmium varies between 9.5 ppm in the Alternation Zone and 150 ppm in the C0 units. In this study, Cd shows a moderate correlation with Zn ($r = 0.73$). In phosphatic level 33, which corresponds to a wide replacement by iron oxides, the contents of Cd and Fe_2O_3 are relatively high. Exceptional concentrations, in samples 29 and 33, disturb the correlation.

Sassi (1974) reported that Cd in phosphorites deposits in Tunisia is associated with Zn. The Cd–Zn association is confirmed by other works (Belayouni and Khamli, 1988; Béji Sassi, 1984; Khamli, 1988; Chaabani, 1995; Béji Sassi and Sassi, 1999). According to these authors, the Cd can be incorporated in part in the apatite lattice but it is mainly contained in sphalerite where it replaces Zn. Indeed, Zn in sphalerite can be partially replaced by Cd because of their very close electronegativity, respectively 1.6 and 1.7 (Klein and Hurlbut, 1993), in spite of the different ionic radii (Zn^{2+} 0.74 Å and Cd^{2+} 0.97 Å).

Electron microprobe analysis of the sphalerite in the phosphate deposits of GMB shows a dispersal of the results across the crystal sphalerite and also throughout the basin (Béji Sassi and Sassi, 1999). Thus, the Zn/Cd ratio found at M'Rata range from 3.8 to 5.1 for 10 sphalerite crystals. Farther South M'Dhilla, this ratio ranges from 7.2 to 14.3. In this study, Zn/Cd ratio varies between 4 (C0-sample 33) and 18.5 (sample 29) with an average of 8.4. These results reflect the dispersal characteristics of the phosphatic series and the various physical and chemical conditions that prevail during diagenesis.

ii) Zirconium, hafnium, barium, uranium and thorium

Compared to Zr values observed in phosphorites by Altschuler (1980), ranging from 13 to 20 ppm, the GMB mineral-bearing rocks show a high content (52–135 ppm) but it is depleted compared to UCC (190 ppm). The lowest content (39–43 ppm), are in the chert level, where P_2O_5 is comprised between 1–1.5%. Also, there is no clear correlation in the Zr–P_2O_5. However, in phosphorites levels, the XRD and the photonic microscopy reveal a small presence of quartzo-feldspatic fraction in which Zr is up to 80 ppm. In the other layers, this element is between 39 and 80 ppm. It may be possible that the volcanic activity during the Paleocene was of explosive-type with ashes and various minerals (Clocchiatti and Sassi, 1972; Sassi, 1974; Béji Sassi *et al.*, 1996). These volcanic events seem to occur either at the beginning or at the end of a phosphatic episod (Sassi, 1974).

Zr is a hydrophilic element; it is enriched in the liquid phase (magma) expelled during violent eruptions. This subaerial Tertiary volcanism of acidic-type could have dispersed the materials in the different phosphatic basins. Glass alteration, in the marine environment, releases Zr and explains the excess Zr found in the phosphorites layers, which also contain a small fraction of quartz and feldspars from volcanic ashes.

The positive correlation between Zr and U (0.79) may be related to CFA. Although the replacement of Ca^{2+} (ionic radius 1.12 Å) by Zr^{4+} (ionic radius 0.84 Å), in the structure of the CFA, is difficult explain (Wittacher and Muntus, 1970), because of the difference in their ionic radii. Zr seems nevertheless to be present in the structure of the CFA, adsorbed at the crystals surfaces.

Hafnium concentrations are relatively low (0.29 to 1.91 ppm). There is a weak correlation between Zr and Hf (0.37), which has a close geochemical behavior recognized by many authors. The average Zr/Hf is 122 compared to 32.75 in UCC and 39 in the zircon. A separation of Zr–Hf is noticed leading Hf affinities to others minerals. Thus, Hf correlates positively with Ta (0.85), TiO_2 (0.65), and MgO (0.75), suggesting that it should be embedded with silicate-sediments, like palygorskite and sepiolite.

Barium is characterized by much lower content (27 to 88 ppm) to those of world phosphorites concentrations (350 ppm) (Altschuler, 1980). Despite the fact that Ba and Sr have the same geochemical behavior because of their higher ionic radii, Ba cannot replace Ca in the CFA lattice as Sr. Wesuggest a possible adsorption on the surface or in the central channel apatite lattice.

Barium is in alkali feldspars and plagioclases. The positive correlation of this element with Zr (0.87) can be explained easily if one accepts, for a part, a volcanic origin for the both elements.

Compared to previously published values (40–60 ppm) in other GMB locations (Sassi, 1974; Chaabani, 1995), U ranges from 3.2 ppm in chert layer to 52 ppm (CIX phosphorite layer) along the Oum El Khecheb cross section with average of 24 ppm. Uranium is commonly believed to be easily incorporated into the apatite lattice (Gulbrandsen, 1966; Altschuler, 1980; Slansky, 1980). The moderate correlation between U–P_2O_5 ($r = 0.7$) cannot exclude a mobility of U that maybe leached by infiltrated waters then immobilized in another structure. On the other hand, from the bottom to the top of Oum El Khecheb profile, uranium exhibits similar fluctuations behavior than REE and Th; they are essentially gathered in the apatite lattice.

Thorium contents are variable and low; they range from 1.13 to 18.4 ppm. The lowest values are related to the Upper Phosphates and to B unit (CVII, CVIII and cherts). As reported, this element shows similar fluctuations as U and may replace Ca in the CFA lattice because of their same sizes (about 1.08 Å). In Fig. 6, Th is close to REE, but has a closer correlation with LREE (close ionic radii) than with HREE where ionic radii are smaller.

Th/U Ratios range from 0.04 in the Upper Phosphates to 0.78 in the chert zone with an average of 0.35. Taylor and McLennan (1985), found 3.86 in the UCC, which is about eleven times higher than in our samples. Altschuler (1980) suggested values in the range of 0.06 and 0.12 for sedimentary phosphorites. Belayouni (1983) gives 0.19 to 0.25 in the phosphorites and 1.95 in the cherts of GMB.

iii) Rubidium, arsenic, scandium, cobalt, antimony, cesium, tantanle and molybdene

The correlation coefficient r (Table 2) of Rb, As, Sc, Co, Sb, Cs, Ta and Mo, with those of silicates as Al_2O_3 and TiO_2 are positive; they are negative with P_2O_5 and Sr. These elements have a similar behavior with those of silicates but are in contradiction with the evolution of the apatite group, and are not in its structure. The presence of these elements in silicates lattice is confirmed by the factor analysis in principal components results (Table 3 and Fig. 6).

Rare Earth Elements Lanthanides REE series are known to be all trivalent with the exception of oxidized Cerium (Ce^{3+}), changing to Ce^{4+}, and Europium (Eu) which acquires the valence II in a reducing environment. Further-

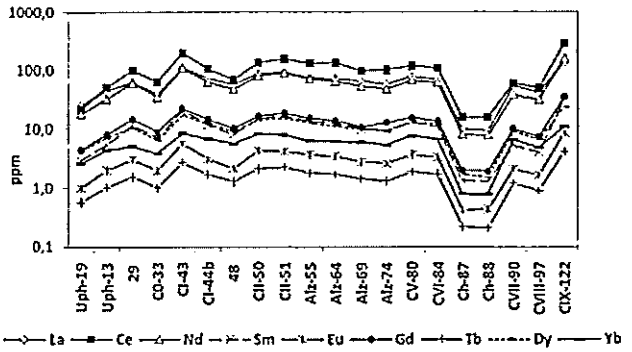

Fig. 10. Rare earth elements distribution (La, Ce, Nd, Sm, Eu, Gd, Tb, Dy and Yb) along the phosphatic section of Oum El Khecheb (GMB; Tunisia). (Uph: Upper Phosphate; Alz: Alternation Zone and Ch: cherts).

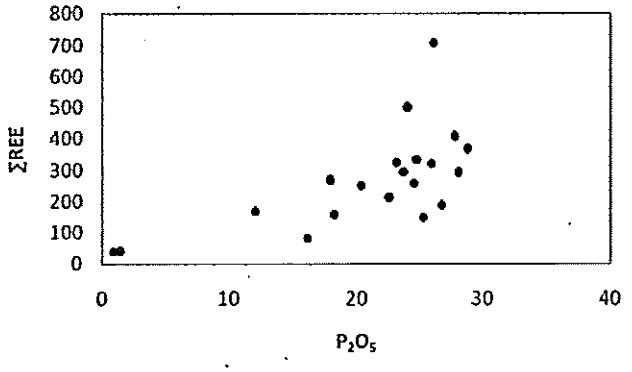

Fig. 11. ΣREE versus P_2O_5 diagram of the Oum El Khecheb phosphorites showing an ordered points cloud.

more, oxidized Cerium is frequently easily hydrolysed, whereas associated minerals, where the oxidized element is contained, are less soluble as CeO_2 has a wide stability field (Eh, pH). In marine environment, this oxidation occurs especially in conjunction with Fe or Mn, phenomenon, which explains its low concentration in seawater (Sholkovitz *et al.*, 1994). However, in this same environment, Eu^{2+} is not easily hydrolysed (Baes and Mesmer, 1976). It exhibits geochemical properties similar to Ca^{2+} and Sr^{2+} and therefore can easily replace them. It changes from its more soluble form to a less soluble form under reducing environments (Eh = –0.4).

Onshore surface waters may contain Eu^{2+}-organic complexes. Furthermore, under anoxic conditions, the reduction of Ce^{4+} to Ce^{3+} occurs and is correlated with sulphides formation as it is reported by Baar *et al.* (1988).

The bulk concentrations of REE abundance are shown in Table 1. The abundances of REE are shown in Fig. 10, where some depletion is observed. It indicates that lanthanide concentrations vary irregularly from the bottom

Table 4. REE contents in some localities of Gafsa Metlaoui Basin (GMB)

Profile	Layer	REE (ppm)	P_2O_5 (%)
Oum El Khecheb	CI	489	24
	CVII	187	26.7
	CVIII	148	25.3
	CIX	705	26.1
Selja (Béji Sassi, 1999)	CI	610	29.2
	CVIII	228	29.2
	CIX	965	29.8
M'Rata (SM 10) (Béji Sassi, 1999)	CI	513	28.5
	CVII	246	27.7
	CVIII	208	24.6
Shale (Piper, 1974)		204.15	
UCC (Taylor and McLennan, 1985)		135	

to the top of the lithostratigraphic column (Fig. 3). The REE percentage does not increase with the P_2O_5 content because the correlation coefficient P_2O_5 varies differently with each REE (Table 2). Thus, it is 0.58 with Sm and Yb with 0.87. It seems therefore that there is a competition between the different REE into the apatite lattice (Fig. 11). Overall, the REE content does not depend solely on P_2O_5 but also varies according to the internal porosity of the grains (Béji Sassi, 1999; Béji Sassi *et al.*, 2005; Ounis *et al.*, 2008), the surface available for the exchanges, the supply and the environmental physico-chemical characteristics of the basin.

From bottom to top, a slightly concave shaped curve and a relative stable REE content is observed. But, some discrepancies can be noticed. If we except values of the siliceous poorly phosphatized beds, representative whole rock REE-analyse of phosphorites present total REE ranging from 81 (Upper Phosphates) to 707 ppm (layer CIX), while P_2O_5 varies from 12% (C0) to 29% (C II).

The depleted REE concentrations are observed in the intensive reddish C0 layer enriched with iron oxides and hydroxides (sample 33). The top of the phosphate deposits (Upper Phosphates) is characterized by the lowest lanthanide contents (Table 1). A change in the depositional environment may explain this depletion. Comparatively to these depleted contents, REE concentrations are stable in the middle part of the lithostratigraphic column emphasizing a stability of sedimentation and diagenetic environment.

Comparisons with results providing from some other localities of the same basin (Béji Sassi, 1999) lead to the following remarks (Table 4). We note that the CIX and CI phosphatic beds, which are characterized by a great

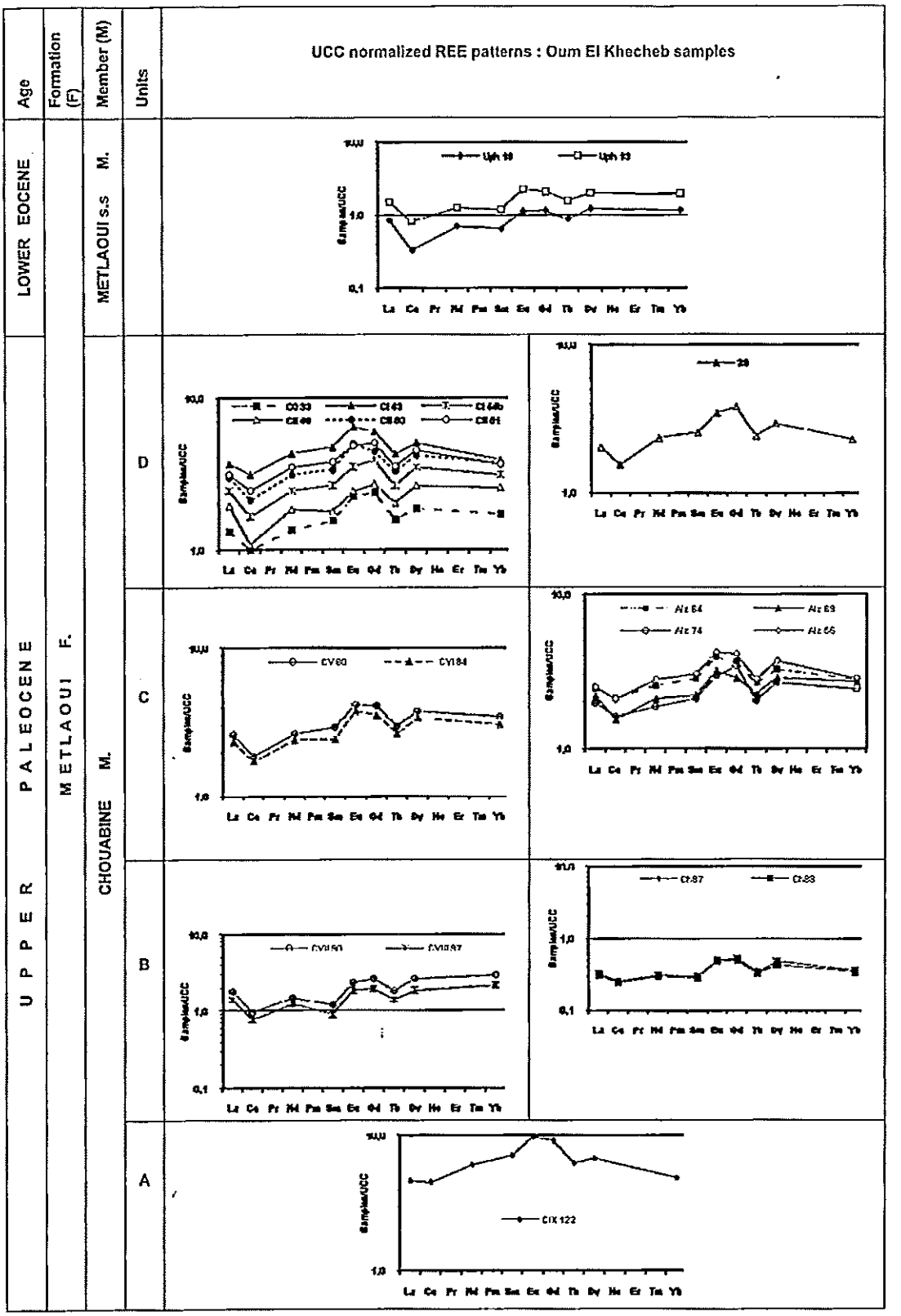

Fig. 12. Rare earth elements normalized to UCC (Upper Continental Crust, after Taylor and McLennan, 1985) of samples of Oum El Khecheb profile.

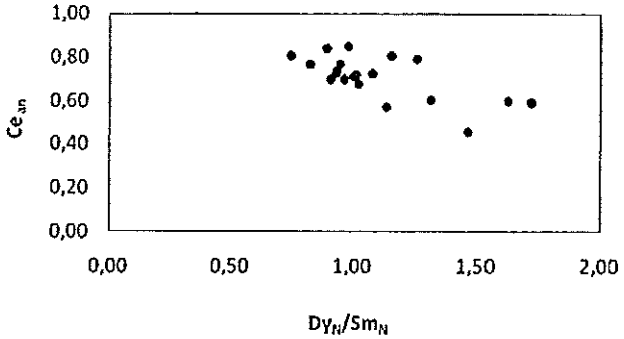

Fig. 13. Ce_{an} versus Dy_N/Sm_N diagram of samples of Oum El Khecheb profile. Dy_N/Sm_N ratio, illustrating the MREE enrichment, shows a negative correlation between the Ce_{an} values.

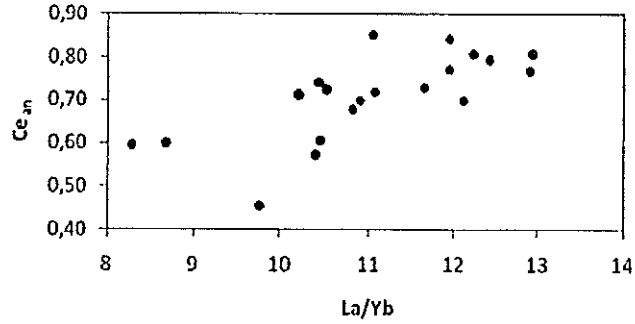

Fig. 15. Ce_{an} versus La/Yb diagram along the phosphatic section of Oum El Khecheb showing a positive correlation between Ce_{an} values and the REE fractionation (La/Yb).

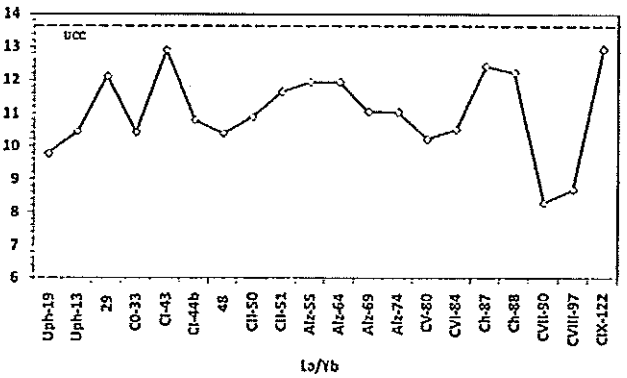

Fig. 14. REE Fractionation expressed by La/Yb along the Oum El Khecheb series.

reworking because of the high degree of the energy in the sedimentary basin and the buried and bioturbated sediments, exhibit the highest REE content. At the same time, CVII and CVIII beds show a REE-content close to the shales values (Piper, 1974) and the UCC (Taylor and McLennan, 1985). CVII and CVIII do not show important reworking marks; their REE supply was stopped with their prompt burial mechanism by the cherty sediments and by the short early diagenesis processes.

If we extend the observations to other localities in the GMB, it appears that the B Unit (CVII and CVIII) is the poorest in rare earth elements while the units A (CIX) and D (CI) are the most enriched ones. REE concentrations mainly relate to the available REE content of the pore fluid. This distribution expresses, on the basin scale, a stable environment and a permanent condition during the phosphate deposition.

We choose to normalize the phosphorites REE contents to the Upper Continental Crust (UCC) (Taylor and McLennan, 1985), as shown in Fig. 12. The normalized REE values range from 1 to 10, which, in other term, mean that they are one-to-ten-times higher than UCC. In the Upper Phosphates, the values are close to the UCC. The REE patterns in both cherts unit are the lowest of the different graphics (Fig. 12). Among the first to use the Ce-anomaly, there are Goldberg *et al.* (1963). It then was used by many other authors (i.e., Elderfield and Greaves, 1981, 1982; De Baar *et al.*, 1985; and most recently Pattan *et al.*, 2005). The REE-anomaly of a given element is defined as the ratio between the measured normalized-value and the value interpolated from the adjacent neighbour normalized-values:

$$\text{Ce anomaly} = (\text{Ce}/\text{Ce}^*),$$

calculated from

$$\text{Ce}^* = 2/3\text{La}_N + 1/3\text{Nd}_N;\ \text{Ce}/\text{Ce}^* = 3\text{Ce}_N/[2\text{La}_N + \text{Nd}_N],$$

where N refers to the UCC normalization of concentrations (Elderfield *et al.*, 1990). When Ce/Ce* is equal to 1 there is no anomaly. For values lower than 1, it is described as negative and when it is higher than 1 it is described as positive. Similarly, Sm, Eu and Tb anomaly are built the same way $(Sm/Sm^*) = Sm_N/(0.5Nd_N + 0.5Eu_N)$; $(Eu/Eu^*) = Eu_N/(0.5Sm_N) + (0.5Gd_N)$; $(Tb/Tb^*) = Tb_N/(0.5Gd_N) + (0.5Dy_N)$, where N refers to normalization of concentrations against UCC (Table 1).

The phosphorites samples present a slight concave-down shaped REE pattern centred on Eu–Gd. Oum El Khecheb phosphorites reveal initial REE distribution patterns with enrichment in the middle REE (MREE) with light REE (LREE) and heavy REE (HREE) weakly fractionated between Sm and Dy. However, relative HREE enrichment can be seen, except for Cherts levels and CIX units (sample 122), where a slight depletion is observed. Oum El Khecheb REE patterns are similar to those of bell-shaped distribution of Haria Formation phosphates (Maastrichian), Alima Mountain (GMB) (Ounis *et al.*,

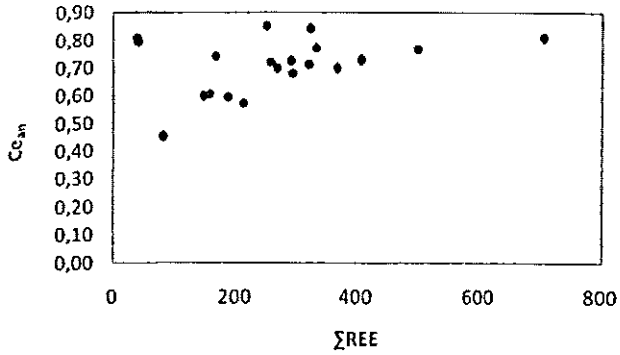

Fig. 16. Ce_{an} versus ΣREE diagram of samples of Oum El Khecheb profile showing positive correlation between the cerium anomaly values and the total REE.

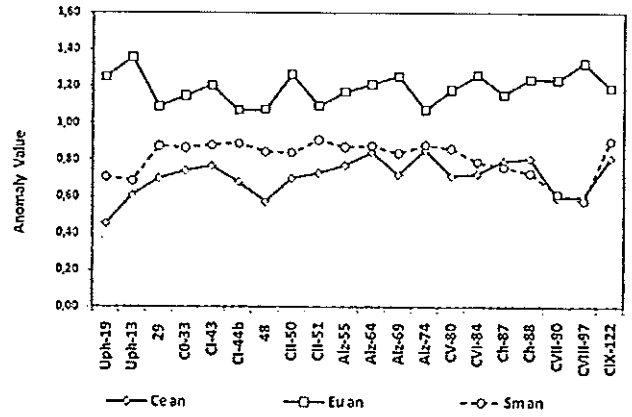

Fig. 17. Ce, Eu and Sm anomalies distribution along the Oum El Khecheb phosphorites profile.

2008). But, REE patterns of Chouabine member (Alima) have a less pronounced MREE enrichment comparatively to analogous Oum el Khecheb phosphorites.

In some samples of Oum ElKhecheb, REE patterns have a tendency towards MREE arching, which may indicate a MREE enrichment. Shields and Stille (2001) used the Dy_N/Sm_N ratio to quantify this arching effect. This ratio is normally above unity in seawater and becomes close to 2 with increasing depth of the water column (Piepgras and Jacobsen, 1992). At Oum El Khecheb, these ratio values range from 0.96 (CIX), and 2.2 (CVII) (Table 1). CVII–CVIII, where REE patterns do not show a clear hat-shape, have the higher ratio value (up to 2).

The cerium anomaly (Ce_{an}) versus Dy_N/Sm_N implies that the concave-down shape of the REE patterns is linked to the intensity of the Ce_{an} (Fig. 13). A clear proportionality exists between Ce-anomaly and MREE enrichment as it is shown by Dy_N/Sm_N.

Three negative Ce, Sm, and Tb-anomalies, plus, possibly, a weak positive Eu-anomaly are observed (Fig. 12). This figure reveals that the phosphates in the mineralized main layers, that the alternations and that the cherts have similar distribution curves respectively, proving similar characters between each samples from those three deposit types.

The fractionation Light-REE/Heavy-REE is expressed by the ratio La/Yb (Grandjean-Lecuyer *et al.*, 1993) (Fig. 14). In this study, La/Yb ratio confirms this fractionation. It is comprised between 8.3 in CVII where Ce_{an} is great (0.6) and 13 in CIX where Ce_{an} is very low (0.81). Note that La/Yb is lower than UCC (13.64). The samples are globally enriched in Heavy-REE. This enrichment correlates positively with the cerium anomalies and reflects the marine water column characteristics (Fig. 15).

The samples throughout the lithostratigraphic column exhibit typical and well pronounced Ce-anomalies. The Upper Phosphates, sample 48 between CI and CII and at the bottom in CVII–CVIII illustrate a typical marine Ce-anomaly. The saw-tooth curve of this value along the profile shows that it is less than 1 (0.45 for Upper Phosphates to 0.85 in the Alternations Zone (74)).

Samples with negative Ce-anomalies indicate that these phosphates have been formed in suboxic environments deficient in this element. It is an anomaly with variable values. It subsides for some samples suggesting a local enrichment, due to a more reducing environment and to humic acids (Froelich *et al.*, 1988; Watkins *et al.*, 1995).

In such environments, Ce is subsequently available, and becomes incorporated into the apatite lattice. Thus the CIX unit, with a reduced negative cerium anomaly (0.9), represents highly reworked phosphorites. The Upper Phosphates are also strongly reworked, and are also characterized by an important negative Ce-anomaly. Where there is no terrigenous input, the Ce-anomaly variations along the Oum El khecheb series reflects the local Eh changes during diagenesis. Except for samples 87 and 88, the cerium anomaly appears to be coupled with the REE abundance represented by the relationship between the Ce_{an} versus ΣREE (Fig. 16). A trend of decreasing Ce-anomaly values with increasing SiO_2 concentration is seen in the chert deposits, possibly due to the organic matter content providing from the Diatoms.

A systematic negative Tb anomaly (0.7) is observed in all the samples. Such anomaly has also been observed in the GMB by Tlig *et al.* (1987); Béji Sassi (1999) and Ounis *et al.* (2008). We believe that the anomaly is not real, but instead, due to the UCC normalization. It seems that there is a problem with the analytical method for Tb and Gd (Brookins, 1989; Elderfield and Greaves, 1982; Taylor and McLennan, 1985; McLennan, 1989). Brookins (1989) believes the terbium anomaly, if real, to be due to other causes than the traditionally evoked for Ce and Eu, which are caused by redox mechanisms.

Also De Baar *et al.* (1985) proposed that the behaviour of Gd^{3+}, due to its special electronic configuration in water, may be slightly different from its neighbours Eu^{3+} and Tb^{3+}. In accordance with that Brookins (1989) proposed for Eu, Gd and Tb, Sm negative anomaly found in the phosphorites is probably due to its electronic configuration. Except for the CIX, Sm anomaly (Sm_{an}) decreases from the bottom to the top of the series (CVIII: 0.58 to CI: 0.88). Sm_{an} evolution in the main phosphatic layers is similar to Ce_{an}. It seems that Ce and Sm obey the same physico-chemical process during the genesis and diagenesis stages. UCC-normalized REE patterns appear to exhibit weak positive Eu anomalies, ranging from 1.1 and 1.3 (Fig. 17). It is known that Eu^{2+} is less soluble under these reduced conditions due to the presence of organic matter. Positive Eu anomalies have been reported in sedimentary phosphorites. McArthur and Walsh (1984) found that Ce_{an} and Eu_{an} have an opposite evolution. This phenomenon may result from a deposition under less oxic conditions during extreme marine diagenesis in certain organic-rich, sulphate reducing environments (MacRae *et al.*, 1992; Shields and Stille, 2001; Stalder and Rozendaal, 2004). Furthermore, the degradation of the organic matter (humic acid) leads to a decrease of the europium-humate complexation constant. Europium is reduced to the divalent state; Eu^{2+} can replace easily Ca^{2+} and Sr^{2+} in the apatite lattice (Monsallier *et al.*, 2001). In the same basin (GMB), Ounis *et al.* (2008) observed for coprolites and teeth a positive Eu_{an} associated with a Ce_{an} ranging from 0.63 to 0.83. REE patterns also show a very weak Tb-negative anomaly.

Conclusions

During the Upper Paleocene–lower Eocene, the Gafsa–Metlaoui Basin was an ideal setting for the phosphatogenesis. Its paleogeography shows two communication pathways with the open sea, and offered a stable neritic sometime restricted conditions to the sedimentation. The arid climate did not change and did not give terrigenous sediments. The subdivision into four units (A, B, C, D) of the Chouabine member in the whole basin indicates a stability and a permanence of the phosphatogenesis progress during the Upper Paleocene. The works reveal that each main phosphatic layer has globally the same characters along the outcrops: the same levels are reworked, or fine-grained or coarse. The nine main phosphatic beds (CI to CIX) have their own characteristics (mineralogical, petrological, and chemical). Our phosphorites are characterized by a francolite-type apatite. It is a sodic, sulphated, fluo-carbonate-apatite, which is relatively rich in REE and strontium. The Phosphatic Series contains calcite, some dolomite and various silicates including aluminous-ferric-magnesian-smectites, palygorskite, and sepiolite. Moreover, a zeolite (clinoptilolite) is present in small quantities. The opal-CT is present in other smaller units that alternate with the phosphatic layers.

During the phosphatogenesis, a contemporary volcanism occurred. In the sediments, a small fraction of quartz and feldspars are remnants of volcanic ashes. The depositional environment of phosphorites is sub-oxic, rich in biogenic organic matter containing humic acids. This basin is characterized by sulphates reduction and the formation of a very small fraction of sulfides (pyrite and sphalerite) and glauconite grains.

The organic productivity is the cause the pre-concentration of phosphorous and REE within the Gafsa–Metlaoui Basin, which is connected to the open sea. Upwelling currents from the Tethys Ocean supplied this basin. These findings on Oum El Khecheb are consistent with the previously established conclusions by Sassi (1974, 1980); Chaabani (1978, 1995) and Belayouni (1983).

The apatite lattice is very favourable for cationic and anionic substitutions. The REE affinity to the mineral is well known. Not all the REE is incorporated into the lattice at the same rate; thus the distribution graphs show several anomalies, some of which are unexplained, such as samarium and terbium. REE abundance in phosphatic grains will reflect their concentration in the genesis marine waters. A further enrichment can occur during diagenesis. Oum El Khecheb phosphorites have REE patterns characterized by variable negative Ce anomaly, indicating a genesis in marine environment deficient in this element. Changes in the anomaly value reflect changes in the Eh-ph environment that lead to the release of the previously-locked cerium and may have caused a slightly positive Europium anomaly.

Acknowledgments—This paper has been greatly benefited by the constructive and encouraging comments and suggestions by the two reviewers Dr. L. Kocsis and Prof. F. Pirajno and Editor Dr. F. Claeys. Thanks are due to Dr. A. Mabrouk for her improvement of the English version.

References

Altschuler, Z. S. (1980) The geochemistry of trace elements in marines phosphorites. Part I. characteristic abundances and enrichment. *Soc. Econ. Paleontal. Mineral. Spec. Publ.* **29**, 19–30.

Altschuler, Z. S., Clarke, R. S. and Young, E. J. (1958) Geochemistry of Uranium in apatite and phosphorites. *U.S. Geol. Surv. Prof. Paper* **314-D**, 45–90.

Altschuler, Z. S., Berman, S. and Cutitta, F. (1967) Rare earth in phosphorites, Geochemistry and potential recovery. *U.S. Geol. Surv. Prof. Paper* **575-B**, 1–9.

Baar, H. J. W., German, C. R., Elderfield, H. and van Gaans, P.

(1988) Rare earth element distribution in anoxic waters of the Cariaco Trench. *Geochim. Cosmochim. Acta* 52, 1203–1219.

Baes, C. F., Jr. and Mesmer, R. E. (1976) *The Hydrolysis of Cations*. Wiley.

Béji Sassi, A. (1984) Pétrologie, Minéralogie et Géochimie des sédiments phosphatés de la bordure orientale de l'île de Kasserine (Tunisie). Thèse Doct. 3ème Cycle, Univ. El Manar, Tunis, 210 pp.

Béji Sassi, A. (1999) Les phosphates dans les bassins paléogènes de la partie méridionale de l'Axe Nord-Sud. (Tunisie). Thèse Doct. d'Etatès-Sci., Univ. Tunis.

Béji Sassi, A. and Sassi, S. (1999) Le cadmium associé aux dépôts phosphatés de la Tunisie méridionale. *J. African Earth Sci.* 29, 501–513.

Béji Sassi, A., Laridhi Ouazaa, N. and Clocchiatti, R. (1996) Les inclusions vitreuses des ilménites, apatites et quartz des sédiments phosphatés de Tunisie: témoignage d'un volcanisme alcalin d'âge paléocène supérieur à éocène. *Bull. Soc. Géol. France* 167(2), 227–234.

Béji Sassi, A., Zaïer, A., Joron, J. L. and Treuil, M. (2005) Rare Earth Elements distribution of Tertiary Phosphorites in Tunisia. *Mineral Deposit Research: Meeting the Global Challenge*, 2, 1061–1064.

Belayouni, H. (1983) Etude de la matière organique dans la série phosphatée du bassin de Gafsa–Métlaoui (Tunisie) Application à la compréhension des mécanismes de la phosphatogenése. Thèse de Doct. ès-Sci., Univ. d'Orlans.

Belayouni, H. and Khamli, N. (1988) Fractionation of some trace elements between apatite and humic acids in phosphate pebbles. *IGCP-156*, Phosphorite, Oxford.

Belayouni, H., Fauconnier, D., Slansky, M. and Trichet, J. (1982) Etude du contenu organique des dépôts phosphatés du bassin de Gafsa. Doc. du B.R.G.M., 35, 70 pp.

Ben Abdesslem, S. (1979) Etude palynologique et micropaléontologique de la série phosphatée du bassin de Gafsa–Métlaoui, Tunisie. Thèse de Doct. Spécialité, Univ. Paris VI.

Bliskovsky, V. Z., Mineyev, D. A. and Kolodov, V. N. (1969) Accessory lanthanides in phosphorites. *Geochim. Int.* 6(6), 1055–1069.

Brookins, G. G. (1989) Aqueous geochemistry of rare earth elements. *Geochemistry and Mineralogy of Rare Earth Elements* (Lipin, B. R. and McKay, G. A., eds.), 221–225, *Min. Soc. Am. Rev. Mineral.* 21.

Chaabani, F. (1978) Les phosphorites de la coupe-type de Foum Selja (Métlaoui, Tunisie), une série sédimentaire séquentielle à évaporites du Paléogène. Thèse 3ème Cycle, Univ. Louis Pasteur, Strasbourg, 131 pp.

Chaabani, F. (1995) Dynamique de la partie orientale du bassin de Gafsa au Crétacé et au Paléogène. Etude minéralogique et géochimique de la série phosphatée éocène. Tunisie méridionale. Thèse Doct. d'état ès-Sci. Univ., Tunis II.

Clocchiatti, R. and Sassi, S. (1972) Découverte de témoins d'un volcanisme paléocène à éocène dans le bassin phosphaté de Métlaoui (Tunisie Méridionale). *C.R. Acad. Sci. Paris* 247, 513–517.

Coque, R. (1958) Morphologie de la Tunisie présaharienne. *Trav. Inst. Rech. Sah., t.* XVII.

Dalirau, F. (2002) Kiruna-type iron oxides apatite ores and "apatite" of the Bafg District, Iran, with an emphasis on the REE geochemistry of their apatite. *Hydrothermal Iron Oxide Copper and Related Deposits: A Global Perspective*, Vol. 2, 303–320, PGC Publishing, Aldelaide.

De Baar, H. J. W., Brewer, P. G. and Bacon, M. P. (1985) Anomalies in rare earth distributions in seawater: Gd and Tb. *Geochim. Cosmochim. Acta* 49, 1961–1969.

Elderfield, H. and Greaves, M. J. (1981) Negative cerium anomalies in the rare earth element patterns of oceanic ferromanganese nodules. *Earth Planet. Sci. Lett.* 55, 163–170.

Elderfield, H. and Greaves, M. J. (1982) The rare earth elements in seawater. *Nature (London)* 296, 214–219.

Elderfield, H., Upstill-Goddard, R. and Sholkovitz, E. R. (1990) The rare earth elements in rivers, estuaries, and coastal seas and their significance to the composition of ocean waters. *Geochim. Cosmochim. Acta* 54, 971–991.

Fleet, M. E. and Pan, Y. (1997) Site preference of rare earth elements in fluorapatite: Binary (LREE + HREE)-substituted crystals. *American Mineralogist* 82, 870–877.

Froelich, P. N., Arthur, M. A., Burnett, W. C., Deakin, M., Hensley, V., Jahnke, R., Kaul, L., Kim, K.-H., Roe, K., Soutar, A. and Vathakanon, C. (1988) Early diagenesis in organic matter in Peru continental margin sediments: Phosphorite precipitation. *Mar. Geol.* 80, 309–343.

Gnandi, K. and Tobschall, H. (2003) Distribution patterns of rare earth elements and uranium in tertiary sedimentary phosphorites of Hahotoé-Kpogamé, Togo. *J. African Earth Sci.* 37, 1–10.

Goldberg, E. D., Koide, M., Schmitt, R. A. and Smith, R. H. (1963) Rare Earth distributions in the marine environment. *J. Geophys. Res.* 68, 4209–4217.

Grandjean-Lecuyer, P., Feist, R. and Albarede, F. (1993) Rare earth elements in old biogenic apatites. *Geochim. Cosmochim. Acta* 57, 2507–2514.

Gulbdransen, R. A. (1966) Chemical composition of phosphorites of the phosphoria Formation. *Geochim. Cosmochim. Acta* 30, 769–778.

Iqdari, A., Velde, B., Benalioulhaj, N., Dujan, S. C. and Yamine, N. (2003) Exchange of light rare earth for Ca in apatite. *C.R. Geoscience* 335, 381–390.

Jarvis, I., Burnett, W. C., Nathan, Y., Almbaydain, F. S. M., Attia, A. K. M., Castro, L. N., Flicoteaux, R., Hilmy, M. E., Hussain, V., Quatawnah, A. A., Serjani, A. and Zanin, Y. N. (1994) Phosphorites geochemistry: state-of-the-art and environment cancers. *Eclogae Geologicae Helvetie* 87, 643–700.

Khamli, N. (1988) Distribution de matière organique dans des éléments triés de phosphate. Conséquence sur la distribution de certains éléments traces. Thèse de spécialité, Univ. de Tunis.

Kidder, D. L., Krishnaswamy, R. and Mapes, R. H. (2003) Elemental mobility in phosphatic shale during concretion growth and implications for provenance analysis. *Chem. Geol.* 198, 335–353.

Klein, C. and Hurlbut, C. (1993) *Manual of Mineralogy*. J. Wiley & Sons, Inc., New York, 681 pp.

MacRae, N. D., Nesbitt, H. W. and Kronberg, B. I. (1992) De-

velopment of a positive Eu-anomaly during diagenesis. *Earth Planet. Sci. Lett.* 109, 585–591.

McArthur, J. M. and Walsh, J. N. (1984) Rare earth geochemistry of phosphorites. *Chem. Geol.* 47, 191–220.

McClellan, G. H. (1980) Mineralogy of carbonate fluorapatites. *J. Geol. Soc. London* 137, 675–681.

McClellan, G. H. and Van Kauwenbergh, S. J. (1990) Clay mineralogy of the phosphorites of the Southeastern United States. *Phosphate Deposits from the World: Vol. 3, Genesis of Neogene to Recent Phosphorites* (Riggs, S. R. and Burnett, W. L., eds.), Cambridge University Press, Cambridge.

McKelvey, V. E. (1950) Rare Earths in western phosphate rocks. U.S. Geol. Surv. Trace elements, Memoire, Rep. No. 194.

McLennan, S. M. (1989) REE in sedimentary rocks: Influence of provenance and sedimentary processes. *Rev. Mineral.* 21, 170–199.

Monsallier, J. M., Scherbaum, F. J., Gunnar Buckau, G., Kim, J.-I., Kumke, M. U., Specht, C. H. and Fritz, H. (2001) Influence of photochemical reactions on the complexation of humic acid with europium(III). *Frimmel Journal of Photochemistry and Photobiology A: Chemistry* 138, 55–63.

Nathan, Y. (1984) The mineralogy and geochemistry of phosphorite. *Phosphate Minerals* (Nriagu, J. O. and Moore, P. B., eds.), 257–291 (Chapter 8), Spriger-Verlag, Berlin.

Ounis, A., Kocsis, L., Chaabani, F. and Pfeifer, H.-R. (2008) Rare earth elements and stable isotope geochemistry of phosphorites deposits in the Gafsa Basin, Tunisia. *Palaeogeogr. Palaeoclimatol. Palaeoecol.* 268, 1–18.

Pattan, J. N., Pearce, N. J. G. and Mislankar, P. G. (2005) Constraints in using Cerium-anomaly of bulk sediments as an indicator of paleo bottom water redox environment: A case study from the Central Indian Ocean Basin. *Chem. Geol.* 221, 260–278.

Piepgras, D. J. and Jacobsen, S. B. (1992) The behavior of rare earth elements in seawater: precise determination of variations in the North Pacific water column. *Geochim. Cosmochim. Acta* 56, 1851–1862.

Piper, D. Z. (1974) Rare earth elements in the sedimentary cycle, a summary. *Chem. Geol.* 14, 285–304.

Price, N. B. and Calvert, S. E. (1978) The geochemistry of phosphorites from the Namibian shelf. *Chem. Geol.* 23, 151–170.

Sassi, S. (1962) Contribution à l'étude de la Sebkha Tegdimane et du Chott el Guettar. Thèse Doc. 3ème Cycle, Univ. Paris Sud Orsay.

Sassi, S. (1974) La sédimentation phosphatée au Paléocène dans le sud et le centre Ouest de la Tunisie. Thèse de Doct. d'état ès Sci., Univ. de Paris Sud, Orsay, 300 pp.

Sassi, S. (1980) Contexte paléogéographique des dépôts phosphatés en Tunisie. *Géologie comparée des gisements de phosphates et de pétrole*, Doc. du B.R.G.M., 24, 167–183.

Sassi, S. and Jacob, C. (1972) Découverte de clinoptilolite dans le bassin phosphaté de Métlaoui (Tunisie), *C.R. Acad. Sci. Paris* 274, 1128–1131.

Semenov, E. I., Kholodov, V. N. and Barinsky, R. L. (1962) Terres rares dans les phosphorites. *Geokhimiya* 5, 434–439, traduction du B.R.G.M.

Shields, G. and Stille, P. (2001) Diagenetic constraints on the use of cerium anomalies as palaeoseawater redox proxies: an isotopic and REE study of Cambrian phosphorites. *Chem. Geol.* 175(1–2), 29–48.

Sholkovitz, E. R., Landing, W. M. and Lewis, B. L. (1994) Ocean particle chemistry: The fractionation of rare earth elements between suspended particles and seawater. *Geochim. Cosmochim. Acta* 58, 1567–1579.

Sin'Kova, L. A., Ivanov, V. L. and Filippov, L. V. (1968) An experimental study of the incorporation of rare earth elements in hydroxyl apatite. *Geokhymica* 3, 304–314 (in Russian).

Slansky, M. (1980) Géologie des phosphates sédimentaires. B.R.G.M. 114.

Soudry, D., Ehrlish, S., Yoffe, O. and Nathan, Y. (2002) Uranium oxidation state and related variations in geochemistry of phosphorites from Negev (southern Israel). *Chem. Geol.* 189, 213–230.

Stalder, M. and Rozendaal, A. (2004) Apatite nodules as an indicator of depositional environment Mesoproterozoic Broken Hill-type Gamsberg Zn–Pb deposit, Namaqua Province, South Africa. *Mineral. Dep.* 39, 189–203.

Taylor, St. R. and McLennan, S. M. (1985) *The Continental Crust: Its Composition and Evolution.* Blackwell Publications, Géoscience texts.

Tlig, S., Sassi, A., Belayouni, H. and Michel, D. (1987) Distribution de l'Uranium, du Thorium, du Zirconium, du Hafnium et des Terres Rares (TR) dans les grains de phosphates sédimentaires. *Chem. Geol.* 62, 209–221.

Tooms, J. S. and Summerhayes, C. R. (1968) Phosphatic rocks from the North-West African continental shelf. *Nature (London)* 218, 1241–1242.

Tooms, J. S., Summerhayes, C. R. and Cronan, D. S. (1969) Geochemistry of marine phosphate and manganese deposits. *Oceanogr. Mar. Biol. Ann. Rev.* 7, 49–100.

Visse, L. D. (1952) Genèse des gîtes phosphatés du Sud-Est algéro-tunisien. *XIXème Congr. Intern. Alger, 1ère série*, 27.

Watkins, R. T., Nathan, Y. and Bremner, J. M. (1995) Rare earth elements in phosphorite ans associated sediment from the Namibian and South Africa continental shelves. *Mar. Geol.* 129, 111–128.

Zaïer, A. (1984) Etude stratigraphique et tectonique de la région de Sra Ouartane (Atlas tunisien central). Lithologie, pétrographie et minéralogie de la série phosphatée. Thèse de Doct. 3ème Cycle, Univ. de Tunis El Manar.

Zaïer, A. (1995) La sédimentation phosphatée dans le gisement de Sékarna (Centre Ouest de la Tunisie). 2ème Congr. Nat. Sci. Terre, Tunis.

Zaïer, A. (1999) Evolution tecto-sédimentaire du bassin phosphaté du Centre-Ouest de la Tunisie. Minéralogie, Pétrologie, Géochimie, et genèse des phosphorites. Thèse Doct. d'Etat ès-Sci., Univ. Tunis El Manar.

Zaïer, A., Béji Sassi, A., Sassi, S. and Moody, R. T. J. (1998). Basin evolution and deposition during the Early Palaeogene in Tunisia: Petroleum Geology of North Africa. *Geol. Soc. London. Spec. Publ.* 132, 375–393.